# Theory for Proton-Coupled Energy Transfer

Kai Cui and Sharon Hammes-Schiffer\*

Department of Chemistry, Princeton University, Princeton, NJ 08544, United States

\*Email: shs566@princeton.edu

# Abstract

In the recently discovered proton-coupled energy transfer (PCEnT) mechanism, the transfer of electronic excitation energy between donor and acceptor chromophores is coupled to a proton transfer reaction. Herein, we develop a general theory for PCEnT and derive an analytical expression for the nonadiabatic PCEnT rate constant. This theory treats the transferring hydrogen nucleus quantum mechanically and describes the PCEnT process in terms of nonadiabatic transitions between reactant and product electron-proton vibronic states. The rate constant is expressed as a summation over these vibronic states, and the contribution of each pair of vibronic states depends on the square of the vibronic coupling as well as the spectral convolution integral, which can be viewed as a generalization of the Förster-type spectral overlap integral for vibronic rather than electronic states. The convolution integral also accounts for the common vibrational modes shared by the donor and acceptor chromophores for intramolecular PCEnT. We apply this theory to model systems to investigate the key features of PCEnT processes. The excited vibronic states contribute significantly to the total PCEnT rate constant, and the common modes can either slow down or speed up the process. Because the pairs of vibronic states that contribute the most to the PCEnT rate constant may correspond to spectroscopically dark states, PCEnT could occur even when there is no apparent overlap between the donor emission and acceptor absorption spectra. This theory will assist in the interpretation of experimental data and will guide the design of additional PCEnT systems.

# I Introduction

Excitation energy transfer (EnT) is a fundamental mechanism in photochemistry, where the electronic excitation energy is transferred between donor and acceptor chromophore molecules.<sup>1-4</sup> This process is ubiquitously found in natural photosynthetic systems,<sup>5-10</sup> as well as in molecular aggregates and polymers.<sup>11-16</sup> EnT has also been utilized as a spectroscopic ruler<sup>17,18</sup> to probe protein folding dynamics<sup>19,20</sup> and has been engineered to enhance the light harvesting in dye-sensitized solar cells.<sup>21</sup> A theoretical formulation of singlet-singlet EnT processes was given by Förster in 1948.<sup>22</sup> In Förster theory, the rate constant for EnT is proportional to the overlap integral between the donor emission and the acceptor absorption spectra. Förster theory provides a simple physical interpretation of the EnT process. The excited donor emits a virtual photon and returns to its ground state, and this virtual photon is absorbed by the acceptor, which is excited from its ground state to its excited state (Figure 1a). According to this theory, EnT can only occur if the donor emission is in resonance with the acceptor absorption. In other words, the donor emission and acceptor absorption spectra must overlap.

Although successfully applied to a wide range of systems, Förster theory has some limitations due to the assumptions made in the derivation.<sup>23,24</sup> For example, in Förster theory the exchange interaction between the donor and acceptor is neglected, and a multipole approximation is used for the Coulomb interaction, which leads to a dipole-dipole coupling term that decreases as the inverse sixth-power of the molecular separation.<sup>24,25</sup> Such approximations are only valid when the separation between the donor and acceptor is larger than the molecular size,<sup>26</sup> and the de-excitation/excitation for the donor/acceptor is symmetry- or spin-allowed (i.e., singlet to singlet).<sup>27</sup> Dexter addressed these issues by deriving an expression for dipole-quadrupole coupling and including the exchange interaction for symmetry- or spin-forbidden transitions.<sup>27</sup> Dexter theory for triplet-triplet EnT features the same spectral overlap integral term as in Förster theory, but the exchange coupling decreases exponentially with the molecular separation.

Förster theory also assumes that the solute and solvent degrees of freedom can be decomposed into two independent sets, which are each coupled to only the donor or only the acceptor.<sup>24,25,28</sup> Such an assumption is often not valid for intramolecular EnT, where the donor and acceptor can have common vibrational modes. The influence of the common vibrational modes on intramolecular EnT has been investigated to some extent.<sup>28,29</sup> Other assumptions of the original Förster-Dexter theories include thermally equilibrated initial states, a localized excitation on a single chromophore,

and incoherent transfer. Several studies have extended Förster-Dexter theory to model nonequilibrium,  $^{30,31}$  multichromophoric,  $^{32-36}$  and coherent  $^{33,37-41}$  EnT, as well as EnT in mediums with complex and dispersive dielectric functions.  $^{42}$ 

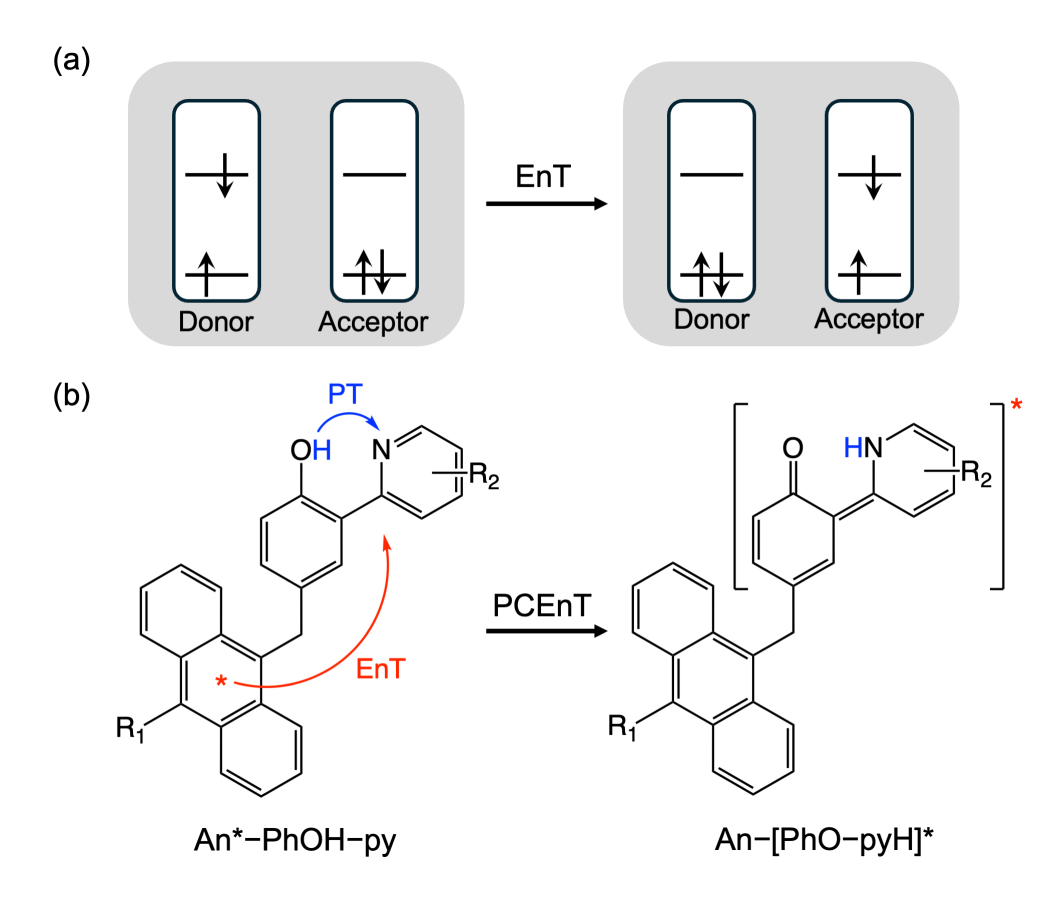


Figure 1: (a) Schematic illustration of a singlet-singlet EnT process, where the electronic excitation energy is transferred from the donor to the acceptor with no charge transfer. (b) PCEnT process discovered in the anthrancene-phenol-pyridine (An–PhOH–py) triad system. The electronic excitation energy is transferred from An to the PhOH–py unit, coupled with proton transfer from PhOH to py.

Recently, a new energy transfer mechanism, called proton-coupled energy transfer (PCEnT), was discovered.<sup>43</sup> In PCEnT, the transfer of electronic excitation energy between chromophores is coupled to a proton transfer reaction. In the anthrancene-phenol-pyridine (An–PhOH–py) triad system (Figure 1b), a local excited state (LES) on the An unit forms upon photoexcitation with 400 nm light. In contrast, direct excitation of the PhOH–py unit requires a much shorter wave length of 330 nm. At 77 K in a butyronitrile glass, the fluorescence spectrum of the triad system excited

at 400 nm contains both the An\* fluorescence, which spans 420 to 580 nm with several structured peaks, and a single broad band with a maximum at around 550 nm, which is assigned to the emission of a local electron-proton transfer (LEPT) state, An–[PhO–pyH]\*. The direct transition from the LES to the LEPT state following photoexcitation was predicted earlier for two of the triads based on excited state dynamics calculations. <sup>44,45</sup> Based on the experimental data, the LEPT state was inferred to form through a PCEnT process, where the electronic excitation energy is transferred from An to the PhOH–py unit, coupled with proton transfer from PhOH to py.

The PCEnT mechanism has several unique properties. Unlike the proton-coupled electron transfer (PCET) process in the triad, where an electron is transferred from PhOH to anthracene, the net charge transfer between the An and the PhOH-py unit is essentially zero throughout the process. Moreover, conventional EnT from An to PhOH-py is prohibitively uphill in energy. The coupled proton transfer lowers the energy of the excited state of PhOH-py and makes energy transfer feasible. It appears that PCEnT can occur when there is no detectable Förster-type spectral overlap between the donor emission and acceptor absorption spectra (i.e., the An emission and PhOH-py absorption spectra). 43 A nonadiabatic surface crossing mechanism was proposed to describe the PCEnT process, where thermal fluctuations of the environment lead to a crossing between the LES and LEPT diabatic electronic states, enabling the electronic energy transfer and proton tunneling to occur simultaneously. 43 However, a rigorous theoretical formulation and an analytical rate constant expression do not yet exist for PCEnT. Note that the term PCEnT was used previously to indicate a different type of mechanisms, where EnT is modulated by the presence of a hydrogen bond 46 or the protonation state of the reactant.<sup>47</sup> In these cases, proton transfer did not occur, in contrast to the mechanism discovered in the triad system, where proton transfer is essential to the electronic energy transfer.

Inspired by the novel PCEnT phenomenon discovered in the triad system, herein we develop an analytical theory for the PCEnT process. In this theory, the energy transfer is described as a nonadiabatic transition between two local excited states, and the transferring proton is treated quantum mechanically. Our group has previously developed a vibronically nonadiabatic PCET theory, <sup>48–51</sup> where the reaction is described in terms of nonadiabatic transitions between reactant and product electron-proton vibronic states. Despite the fundamental physical distinction between PCEnT and PCET processes, the mathematical formulation of the problem (i.e., nonadiabatic transitions between electron-proton vibronic states) is isomorphic. Therefore, an analogous framework can be adopted.

An outline of this paper is as follows. First we introduce the diabatic states involved in the PCEnT process and a model Hamiltonian. Then we use the Fermi golden rule formalism to derive an expression for the PCEnT rate constant in the vibronically nonadiabatic limit. The final expression involves what we call the spectral convolution integral. This can be viewed as a generalization of the Förster-type spectral overlap integral, but the transitions are between electron-proton vibronic states instead of electronic states. Next we apply this theory to a model system to investigate the key features of the PCEnT process. The application to a realistic system (e.g., the triad system) will be the topic of future work. Finally, we discuss how PCEnT could occur when there is no apparent overlap between experimentally measured donor emission and acceptor absorption spectra and discuss the similarities and distinctions between PCEnT and PCET theories.

# II Theory

#### A Model Hamiltonian

We start our derivation with the model Hamiltonian for PCEnT. In a PCEnT process, the excitation energy transfer is coupled with proton transfer (PT). Such a process can be formally expressed as

$$D_{en}^* - D_p - H^+ \cdots A_p - A_{en} \to D_{en} - D_p \cdots + H - A_p - A_{en}^*$$
 (1)

where  $D_{en}$  and  $A_{en}$  represent a general excitation energy donor and acceptor,  $D_{p}$  and  $A_{p}$  represent a general proton donor and acceptor, and H represents the transferring proton. Similar to our theory for PCET<sup>48,49</sup>, we can define four electronic diabatic states involved in this process:

(1a) 
$$D_{en}^* - D_p - H^+ \cdots A_p - A_{en}$$
  
(1b)  $D_{en}^* - D_p \cdots + H - A_p - A_{en}$   
(2a)  $D_{en} - D_p - H^+ \cdots A_p - A_{en}^*$   
(2b)  $D_{en} - D_p \cdots + H - A_p - A_{en}^*$ 

Here a and b denote whether the proton is bonded to its donor or acceptor, respectively, and 1 and 2 denote whether the excitation is localized on the donor or acceptor, respectively. 1a is the initial state of PCEnT, and 2b is the final state of PCEnT.

The relative energies of the four diabatic states typically satisfy the following conditions for PCEnT reactions.<sup>50</sup> The energy of the 1b (2a) state is higher than the energy of the 1a (2b) state so that the proton is more stable on the donor (acceptor) before (after) energy transfer. In addition,

the energy of the 2a (1b) state is higher than the energy of the 1a (2b) state so that the initial and final states correspond to the 1a and 2b states. However, the difference between the energies of the 1a and 2b states could be positive or negative corresponding to an exothermic or endothermic reaction, respectively.

Representing the Hamiltonian using these diabatic states gives a  $4 \times 4$  matrix. It is also useful to define two auxiliary diabatic states, where neither  $D_{\rm en}$  nor  $A_{\rm en}$  is excited:

(Ga) 
$$D_{en}-D_p-H^+ \cdots A_p-A_{en}$$
  
(Gb)  $D_{en}-D_p \cdots +H-A_p-A_{en}$  (3)

where G indicates the ground state. Note that PCEnT is a radiationless process, and therefore Ga and Gb are not actually involved in PCEnT.

Similar to the PCET case,  $^{48,49}$  the electronic coupling between states 1a/1b, 2a/2b, or Ga/Gb is typically large because of the hydrogen-bonding interaction.  $^{49}$  Thus, we will focus on the regime of electronically adiabatic PT within states 1, 2, or the ground state in this paper. We can construct three new electronic states as the following linear combinations of the six diabatic states defined in Eqs. (2) and (3):

$$|I\rangle = C_{1a}|1a\rangle + C_{1b}|1b\rangle$$

$$|II\rangle = C_{2a}|2a\rangle + C_{2b}|2b\rangle$$

$$|G\rangle = C_{Ga}|Ga\rangle + C_{Gb}|Gb\rangle$$
(4)

where the expansion coefficients are determined by block diagonalization of each  $2 \times 2$  Hamiltonian. By construction,  $|G\rangle$  is the electronic adiabatic ground state of the system, and  $|I\rangle$  and  $|II\rangle$  are the electronic diabatic states corresponding to the reactant and product for PCEnT. The electronic wave functions for these states are denoted as  $\psi_j$ , where j = G, I, II.

Considering a PCEnT system embedded in solution, the coordinates of the electrons, the transferring proton, and all other nuclei are denoted as  $r_{\rm e}$ ,  $r_{\rm p}$ , and q, respectively. Here q encompasses all normal mode coordinates of the intramolecular vibrations and the solvent coordinates and hereon will be referred to as the bath coordinate. The total Hamiltonian of the system is

$$\hat{H}(\boldsymbol{r}_{e}, \boldsymbol{r}_{p}, \boldsymbol{q}) = \hat{T}_{e} + \hat{T}_{p} + \hat{T}_{q} + V(\boldsymbol{r}_{e}, \boldsymbol{r}_{p}, \boldsymbol{q})$$
(5)

where  $\hat{T}_{\rm e}$ ,  $\hat{T}_{\rm p}$ , and  $\hat{T}_{q}$  are the kinetic energy operators for the electrons, transferring proton, and bath coordinates, respectively, in the PCEnT system, and V is the potential energy, which includes the solvent-solvent interaction.

To obtain the energies and wave functions of the system, we first separate the electronic degrees of freedom from those of the transferring proton and the bath. The electronic Hamiltonian is

$$\hat{H}_{el}(\mathbf{r}_e; \mathbf{r}_p, \mathbf{q}) = \hat{T}_e + V(\mathbf{r}_e; \mathbf{r}_p, \mathbf{q})$$
(6)

The electronic energy for diabatic state  $|j\rangle$  is

$$E_j(\mathbf{r}_{\mathrm{p}}, \mathbf{q}) = \left\langle \psi_j(\mathbf{r}_{\mathrm{e}}; \mathbf{r}_{\mathrm{p}}, \mathbf{q}) \middle| \hat{H}_{\mathrm{el}} \middle| \psi_j(\mathbf{r}_{\mathrm{e}}; \mathbf{r}_{\mathrm{p}}, \mathbf{q}) \right\rangle$$
(7)

Separating the transferring proton degrees of freedom from those of the bath, the proton vibrational states associated with diabatic state  $|j\rangle$  are given by

$$\left[\hat{T}_{p} + E_{j}(\boldsymbol{r}_{p}; \boldsymbol{q})\right] \chi_{\mu}^{(j)}(\boldsymbol{r}_{p}; \boldsymbol{q}) = E_{j\mu}(\boldsymbol{q}) \chi_{\mu}^{(j)}(\boldsymbol{r}_{p}; \boldsymbol{q})$$
(8)

where  $\mu$  denotes the proton vibrational state, and  $E_{j\mu}$  is the electron-proton vibronic energy that defines the potential energy surface (PES) for the bath. Defining  $\mathbf{q}_{\rm eq}^{(j\mu)}$  as the equilibrium position on the PES corresponding to the vibronic state  $|j\mu\rangle$ , the bath Hamiltonian associated with vibronic state  $|j\mu\rangle$  can be expressed as

$$\hat{H}_{\mathrm{B}}^{(j\mu)}(\boldsymbol{q}) = \hat{T}_{q} + E_{j\mu}(\boldsymbol{q}) - E_{j\mu}(\boldsymbol{q}_{\mathrm{eq}}^{(j\mu)})$$

$$\tag{9}$$

with eigenstates and energies given by

$$\hat{H}_{\mathbf{B}}^{(j\mu)}(\mathbf{q})\Theta_{m}^{(j\mu)}(\mathbf{q}) = \varepsilon_{m}^{(j\mu)}\Theta_{m}^{(j\mu)}(\mathbf{q}) \tag{10}$$

Note that we have not imposed restrictions on the functional form of  $E_{j\mu}(\mathbf{q})$ . Therefore, the bath Hamiltonian in Eq. (9) is able to describe anharmonic solute vibrations, nonlinear solvation effects, and changes of solute polarizability. Such effects have been shown to be important in electron transfer reactions.<sup>52–54</sup>

The total wave function of the system for electronic diabatic state j, proton vibrational state  $\mu$ , and bath state m is

$$\Psi_{j\mu m}(\mathbf{r}_{e}, \mathbf{r}_{p}, \mathbf{q}) = \psi_{j}(\mathbf{r}_{e}; \mathbf{r}_{p}, \mathbf{q}) \chi_{\mu}^{(j)}(\mathbf{r}_{p}; \mathbf{q}) \Theta_{m}^{(j\mu)}(\mathbf{q})$$
(11)

with corresponding total energy

$$E_{j\mu m} = E_{j\mu}(\mathbf{q}_{eq}^{(j\mu)}) + \varepsilon_m^{(j\mu)}$$
(12)

For notational simplicity, from hereon we will simply write  $E_{j\mu}$  to denote  $E_{j\mu}(\mathbf{q}_{eq}^{(j\mu)})$ , which is independent of the bath coordinate  $\mathbf{q}$ .

The coupling between these states is given by the matrix element  $V_{j\mu m,k\nu n} = \langle \Psi_{j\mu m} | \hat{H} | \Psi_{k\nu n} \rangle$ . Applying the Condon approximation, where the vibronic coupling is independent of the bath motion,

$$V_{j\mu m,k\nu n} = V_{j\mu,k\nu} \langle \Theta_m^{(j\mu)} | \Theta_n^{(k\nu)} \rangle \tag{13}$$

Here  $V_{j\mu,k\nu} = \left\langle \psi_j(\boldsymbol{r}_{\mathrm{e}}; \boldsymbol{r}_{\mathrm{p}}, \boldsymbol{q}^*) \chi_{\mu}^{(j)}(\boldsymbol{r}_{\mathrm{p}}; \boldsymbol{q}^*) \left| \hat{H}_{\mathrm{el}} + \hat{T}_{\mathrm{p}} \right| \psi_k(\boldsymbol{r}_{\mathrm{e}}; \boldsymbol{r}_{\mathrm{p}}, \boldsymbol{q}^*) \chi_{\nu}^{(k)}(\boldsymbol{r}_{\mathrm{p}}; \boldsymbol{q}^*) \right\rangle$  is the vibronic coupling, and  $\boldsymbol{q}^*$  represents a set of fixed bath coordinates. Typically  $\boldsymbol{q}^*$  is chosen to be the crossing point between the two diabatic vibronic states.

PCEnT corresponds to the transition between diabatic states  $|I\rangle$  and  $|II\rangle$ . Using the matrix elements calculated above, we obtain the two-level model Hamiltonian for PCEnT:

$$\mathbf{H} = \begin{bmatrix} E_{\mathrm{I}\mu} + \varepsilon_m^{(\mathrm{I}\mu)} & V_{\mathrm{I}\mu,\mathrm{II}\nu} \langle \Theta_m^{(\mathrm{I}\mu)} | \Theta_n^{(\mathrm{II}\nu)} \rangle \\ V_{\mathrm{II}\nu,\mathrm{I}\mu} \langle \Theta_n^{(\mathrm{II}\nu)} | \Theta_m^{(\mathrm{I}\mu)} \rangle & E_{\mathrm{II}\nu} + \varepsilon_n^{(\mathrm{II}\nu)} \end{bmatrix}$$
(14)

In the vibronically nonadiabatic limit, the rate constant can be calculated as a sum over nonradiative transitions between two sets of quantum states using Fermi's golden rule:

$$k_{\text{PCEnT}} = \frac{2\pi}{\hbar} \sum_{\mu,\nu} P_{\text{I}\mu} |V_{\mu\nu}|^2 \sum_{m,n} f(\varepsilon_m^{(\text{I}\mu)}) \left| \langle \Theta_m^{(\text{I}\mu)} | \Theta_n^{(\text{II}\nu)} \rangle \right|^2 \delta(E_{\text{II}\nu} + \varepsilon_n^{(\text{II}\nu)} - E_{\text{I}\mu} - \varepsilon_m^{(\text{I}\mu)})$$
(15)

where  $V_{\mu\nu}$  is the abbreviation for  $V_{\mathrm{I}\mu,\mathrm{II}\nu}$ ,  $P_{\mathrm{I}\mu}$  is the Boltzmann population for the discrete reactant electron-proton vibronic state  $|\mathrm{I}\mu\rangle$ , and  $f(\varepsilon_m^{(\mathrm{I}\mu)})$  is the Boltzmann distribution function for the bath states associated with vibronic state  $|\mathrm{I}\mu\rangle$ , which is assumed to be a quasi-continuum. We also assume that  $P_{\mathrm{I}\mu}$  and  $f(\varepsilon_m^{(\mathrm{I}\mu)})$  are separable within the overall Boltzmann distribution of states for state  $|\mathrm{I}\mu m\rangle$ , i.e.,  $f(E_{\mathrm{I}\mu m}) = P_{\mathrm{I}\mu}f(\varepsilon_m^{(\mathrm{I}\mu)})$ . In other words, the Boltzmann distribution for the bath states is the same for all proton vibrational states  $\mu$ .

Up to this step, we have made the following main approximations: (1) the vibronic coupling between states  $|I\mu\rangle$  and  $|II\nu\rangle$  is small relative to the thermal energy; (2) the bath has quasi-continuum states; (3) the initial state reaches thermal equilibrium with the bath before the transition occurs; (4) the Condon approximation, where the vibronic coupling is independent of the bath motion.  $^{24,25,55}$  Assumptions (1) and (2) ensure the validity of Fermi's golden rule formula, and assumption (3) allows the use of the equilibrium distribution function when calculating the rate constant. In principle, as shown in the development of EnT theories, assumptions (3) and (4) can be lifted, leading to more complicated expressions.  $^{28,30,56}$  Although the golden rule formalism used in this paper neglects electronic coherence, the theories developed for coherent EnT could be extended to describe coherent PCEnT.  $^{33,37-41}$ 

### B General Rate Constant Expression

For any PCEnT process described by Eq. (1), we can partition the total system into two moieties, denoted as D and A. The energy donor is included in moiety D, and the energy acceptor is included in moiety A. Depending on the system of interest, there are multiple possibilities to partition the proton donor and acceptor, such as

$$\underbrace{D_{\text{en}}^*}_{\text{D}} - \underbrace{[D_{\text{p}} - H^+ \cdots A_{\text{p}} - A_{\text{en}}]}_{\text{A}} \rightarrow \underbrace{D_{\text{en}}}_{\text{D}} - \underbrace{[D_{\text{p}} \cdots^+ H - A_{\text{p}} - A_{\text{en}}]^*}_{\text{A}}$$
(16a)

$$\underbrace{[D_{en}-D_p-H^+\cdots A_p]^*}_{D}\underbrace{-A_{en}}_{A}\to \underbrace{[D_{en}-D_p\cdots^+H-A_p]}_{D}-\underbrace{A_{en}^*}_{A}$$
(16b)

$$\underbrace{[D_{en}-D_{p}]^{*}}_{D} - H^{+} \cdots \underbrace{[A_{p}-A_{en}]}_{A} \rightarrow \underbrace{[D_{en}-D_{p}]}_{D} \cdots + H - \underbrace{[A_{p}-A_{en}]^{*}}_{A}$$
(16c)

Note that the transferring proton is quantized and therefore is not considered to be associated with either the donor or the acceptor, analogous to the electrons. The following derivations will be the same regardless of how the proton donor and acceptor are partitioned.

To include both intermolecular and intramolecular PCEnT in a general formula, we assume that most bath modes are coupled only to either the donor D or the acceptor A, and only a few additional modes (e.g., the stretch of the bridge or the twist around the bridge for the triads) are coupled to both moieties. The bath Hamiltonians can thus be decomposed as

$$\hat{H}_{B}^{(I\mu)}(\mathbf{q}) = \hat{H}_{B,D}^{(e_{D}\mu)}(\mathbf{q}_{D}) + \hat{H}_{B,A}^{(g_{A}\mu)}(\mathbf{q}_{A}) + \hat{H}_{B,com}^{(I\mu)}(\mathbf{q}')$$
(17a)

$$\hat{H}_{\rm B}^{({\rm II}\nu)}(q) = \hat{H}_{\rm B,D}^{({\rm g}_{\rm D}\nu)}(q_{\rm D}) + \hat{H}_{\rm B,A}^{({\rm e}_{\rm A}\nu)}(q_{\rm A}) + \hat{H}_{\rm B,com}^{({\rm II}\nu)}(q')$$
(17b)

$$\hat{H}_{\mathrm{B}}^{(\mathrm{G}\sigma)}(\boldsymbol{q}) = \hat{H}_{\mathrm{B},\mathrm{D}}^{(\mathrm{g}_{\mathrm{D}}\sigma)}(\boldsymbol{q}_{\mathrm{D}}) + \hat{H}_{\mathrm{B},\mathrm{A}}^{(\mathrm{g}_{\mathrm{A}}\sigma)}(\boldsymbol{q}_{\mathrm{A}}) + \hat{H}_{\mathrm{B},\mathrm{com}}^{(\mathrm{G}\sigma)}(\boldsymbol{q}')$$
(17c)

Here q' denotes the generalized coordinates of the common modes, which are also indicated by the "com" subscript on the Hamiltonians.  $\hat{H}_{B,D}$ ,  $\hat{H}_{B,A}$ , and  $\hat{H}_{B,com}$  mutually commute because Hamiltonians for different coordinates commute. With this decomposition, the bath Hamiltonian associated with moiety D becomes independent of the electronic state of moiety A and *vice versa*. The electronic states for  $\hat{H}_{B,D}$  and  $\hat{H}_{B,A}$  are thus labeled according to whether the donor is in its ground or excited state ( $g_D$  or  $e_D$ ) and whether the acceptor is in its ground or excited state ( $g_A$  or  $e_A$ ) instead of I and II. The index  $\sigma$  denotes the proton vibrational state associated with electronic state  $|G\rangle$ .

The wave functions and energies associated with the bath can also be decomposed:

$$\Theta_m^{(\mathrm{I}\mu)}(\boldsymbol{q}) = \Theta_{m_1}^{(\mathrm{e}_{\mathrm{D}}\mu)}(\boldsymbol{q}_{\mathrm{D}})\Theta_{m_2}^{(\mathrm{g}_{\mathrm{A}}\mu)}(\boldsymbol{q}_{\mathrm{A}})\Theta_{m_2}^{(\mathrm{I}\mu)}(\boldsymbol{q}')$$
(18a)

$$\Theta_n^{(\mathrm{II}\nu)}(\boldsymbol{q}) = \Theta_{n_1}^{(\mathrm{g}_\mathrm{D}\nu)}(\boldsymbol{q}_\mathrm{D})\Theta_{n_2}^{(\mathrm{e}_\mathrm{A}\nu)}(\boldsymbol{q}_\mathrm{A})\Theta_{n_3}^{(\mathrm{II}\nu)}(\boldsymbol{q}')$$
(18b)

$$\Theta_l^{(G\sigma)}(\boldsymbol{q}) = \Theta_{l_1}^{(g_D\sigma)}(\boldsymbol{q}_D)\Theta_{l_2}^{(g_A\sigma)}(\boldsymbol{q}_A)\Theta_{l_3}^{(G\sigma)}(\boldsymbol{q}')$$
(18c)

$$\varepsilon_m^{(\text{I}\mu)} = \varepsilon_{m_1}^{(\text{e}_{\text{D}}\mu)} + \varepsilon_{m_2}^{(\text{g}_{\text{A}}\mu)} + \varepsilon_{m_3}^{(\text{I}\mu)}$$
(19a)

$$\varepsilon_n^{(\text{II}\nu)} = \varepsilon_{n_1}^{(\text{g}_\text{D}\nu)} + \varepsilon_{n_2}^{(\text{e}_\text{A}\nu)} + \varepsilon_{n_3}^{(\text{II}\nu)} \tag{19b}$$

$$\varepsilon_l^{(G\sigma)} = \varepsilon_{l_1}^{(g_D\sigma)} + \varepsilon_{l_2}^{(g_A\sigma)} + \varepsilon_{l_3}^{(G\sigma)} \tag{19c}$$

The delta function in Eq. (15) becomes

$$\delta(\dots) = \delta(E_{\text{II}\nu} + \varepsilon_{n_1}^{(\text{g}_{\text{D}}\nu)} + \varepsilon_{n_2}^{(\text{e}_{\text{A}}\nu)} + \varepsilon_{n_3}^{(\text{II}\nu)} - E_{\text{I}\mu} - \varepsilon_{m_1}^{(\text{e}_{\text{D}}\mu)} - \varepsilon_{m_2}^{(\text{g}_{\text{A}}\mu)} - \varepsilon_{m_3}^{(\text{I}\mu)}$$

$$+ E_{\text{G}\sigma} - E_{\text{G}\sigma})$$

$$= \hbar^2 \iint d\omega_1 d\omega_2 \, \delta(E_{\text{G}\sigma} + \varepsilon_{n_1}^{(\text{g}_{\text{D}}\nu)} - E_{\text{I}\mu} - \varepsilon_{m_1}^{(\text{e}_{\text{D}}\mu)} + \hbar\omega_1)$$

$$\times \delta(E_{\text{II}\nu} + \varepsilon_{n_2}^{(\text{e}_{\text{A}}\nu)} - E_{\text{G}\sigma} - \varepsilon_{m_2}^{(\text{g}_{\text{A}}\mu)} - \hbar\omega_2)$$

$$\times \delta(\varepsilon_{n_3}^{(\text{II}\nu)} - \varepsilon_{m_3}^{(\text{I}\mu)} - \hbar(\omega_1 - \omega_2))$$

$$(20)$$

In the first line we added and subtracted the same quantity,  $E_{G\sigma}$ , which is the energy of the vibronic state corresponding to the electronic ground state and proton vibrational state  $\sigma$ . Here  $|G\sigma\rangle$  is just an auxiliary state used to simplify the mathematical expression and is not involved in the actual PCEnT process. Furthermore, the manipulation of the delta function in Eq. (20) is independent of the choice of  $\sigma$ . For simplicity, we will set  $\sigma = 0$ .

Eq. (20) expresses the original delta function in Eq. (15) as a double integral of three delta functions. The first term contains an energy difference  $E_{\rm G0} - E_{\rm I\mu}$  (setting  $\sigma = 0$ ), which corresponds to the de-excitation from vibronic state  $|{\rm I}\mu\rangle$  to  $|{\rm G0}\rangle$  (donor emission). The second term contains an energy difference  $E_{\rm II}\nu - E_{\rm G0}$ , which corresponds to the excitation from vibronic state  $|{\rm G0}\rangle$  to  $|{\rm II}\nu\rangle$  (acceptor absorption). We define the following transition frequencies:

$$\omega_{\mu 0}^{\text{eq,D}} = \frac{E_{\text{I}\mu} - E_{\text{G}0}}{\hbar} \tag{21a}$$

$$\omega_{0\nu}^{\text{eq,A}} = \frac{E_{\text{II}\nu} - E_{\text{G0}}}{\hbar} \tag{21b}$$

Note that we are defining the transition frequencies in a way that they are always greater than zero, regardless of whether the process is emission or absorption.  $\omega_{\mu 0}^{\text{eq,D}}$  and  $\omega_{0\nu}^{\text{eq,A}}$  will be referred to as equilibrium transition frequencies because the energies  $E_{\text{I}\mu}$ ,  $E_{\text{II}\nu}$ , and  $E_{\text{G0}}$  are evaluated when the bath coordinates are at their equilibrium positions on the corresponding vibronic states (i.e.,

at each individual vibronic state). These should not be confused with the vertical (Frank-Condon) transition frequencies,  $\omega_{\mu 0}^{\perp, D}$  and  $\omega_{0\nu}^{\perp, A}$ , where the nuclear positions are fixed at the equilibrium positions of the *initial* state:

$$\omega_{\mu 0}^{\perp,D} = \frac{E_{I\mu}(\mathbf{q}_{eq}^{(I\mu)}) - E_{G0}(\mathbf{q}_{eq}^{(I\mu)})}{\hbar} = \omega_{\mu 0}^{eq,D} - \frac{E_{G0}(\mathbf{q}_{eq}^{(I\mu)}) - E_{G0}(\mathbf{q}_{eq}^{(G0)})}{\hbar} \equiv \omega_{\mu 0}^{eq,D} - \frac{\lambda_{\mu 0}^{D}}{\hbar}$$
(22a)

$$\omega_{0\nu}^{\perp,A} = \frac{E_{\text{II}\nu}(\boldsymbol{q}_{\text{eq}}^{(\text{G0})}) - E_{\text{G0}}(\boldsymbol{q}_{\text{eq}}^{(\text{G0})})}{\hbar} = \omega_{0\nu}^{\text{eq,A}} + \frac{E_{\text{II}\nu}(\boldsymbol{q}_{\text{eq}}^{(\text{G0})}) - E_{\text{II}\nu}(\boldsymbol{q}_{\text{eq}}^{(\text{II}\nu)})}{\hbar} \equiv \omega_{0\nu}^{\text{eq,A}} + \frac{\lambda_{0\nu}^{\text{A}}}{\hbar}$$
(22b)

where  $\lambda_{\mu 0}^{\rm D} = E_{\rm G0}(\boldsymbol{q}_{\rm eq}^{({\rm I}\mu)}) - E_{\rm G0}(\boldsymbol{q}_{\rm eq}^{({\rm G0})})$  is the reorganization energy for donor emission, and  $\lambda_{0\nu}^{\rm A} = E_{\rm II\nu}(\boldsymbol{q}_{\rm eq}^{({\rm G0})}) - E_{\rm II\nu}(\boldsymbol{q}_{\rm eq}^{({\rm II}\nu)})$  is the reorganization energy for acceptor absorption. These definitions are schematically illustrated in Figure 2.

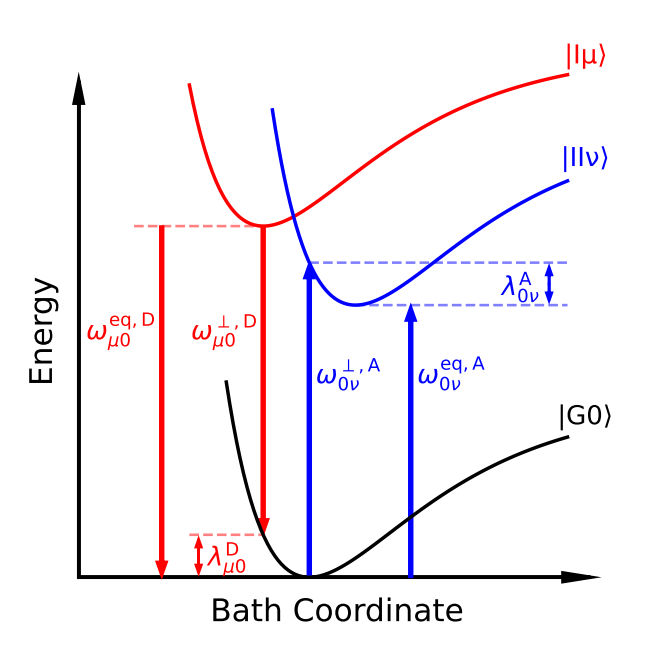


Figure 2: Schematic illustration of the electron-proton vibronic potential energy surfaces as functions of the bath coordinate  $\boldsymbol{q}$ . The transition frequencies  $\omega_{\mu 0}^{\text{eq,D}}$ ,  $\omega_{0\nu}^{\text{eq,A}}$ ,  $\omega_{\mu 0}^{\perp,D}$ , and  $\omega_{0\nu}^{\perp,A}$  are indicated by single-headed arrows, and  $\lambda_{\mu 0}^{\text{D}}$  and  $\lambda_{0\nu}^{\text{A}}$  are indicated by double-headed arrows. Note that the x-axis could be viewed as a collective bath coordinate, and the curves could be computed as the potential of mean force along this collective bath coordinate, in which case the y-axis would be free energy.

Using these definitions and the delta function in Eq. 20, the summation over m and n in Eq. (15)

becomes

$$\sum_{m,n} \dots = \hbar^{2} \iint d\omega_{1} d\omega_{2} \left( \sum_{m_{1},n_{1}} f(\varepsilon_{m_{1}}^{(e_{D}\mu)}) \left| \langle \Theta_{m_{1}}^{(e_{D}\mu)} | \Theta_{n_{1}}^{(g_{D}\nu)} \rangle \right|^{2} \delta(\varepsilon_{n_{1}}^{(g_{D}\nu)} - \varepsilon_{m_{1}}^{(e_{D}\mu)} + \hbar(\omega_{1} - \omega_{\mu 0}^{eq,D})) \right) \\
\times \left( \sum_{m_{2},n_{2}} f(\varepsilon_{m_{2}}^{(g_{A}\mu)}) \left| \langle \Theta_{m_{2}}^{(g_{A}\mu)} | \Theta_{n_{2}}^{(e_{A}\nu)} \rangle \right|^{2} \delta(\varepsilon_{n_{2}}^{(e_{A}\nu)} - \varepsilon_{m_{2}}^{(g_{A}\mu)} - \hbar(\omega_{2} - \omega_{0\nu}^{eq,A})) \right) \\
\times \left( \sum_{m_{3},n_{3}} f(\varepsilon_{m_{3}}^{(I\mu)}) \left| \langle \Theta_{m_{3}}^{(I\mu)} | \Theta_{n_{3}}^{(II\nu)} \rangle \right|^{2} \delta(\varepsilon_{n_{3}}^{(II\nu)} - \varepsilon_{m_{3}}^{(I\mu)} - \hbar(\omega_{1} - \omega_{2})) \right) \tag{23}$$

The formula in each parenthesis closely resembles the definition of line shape functions in the theory for optical absorption and emission.<sup>25</sup> The difference is that here the transitions are between vibronic states instead of electronic states. We can define the line shape functions  $L_{\mu\nu}^{\rm D,em}(\omega_1 - \omega_{\mu 0}^{\rm eq,D})$  and  $L_{\mu\nu}^{\rm A,abs}(\omega_2 - \omega_{0\nu}^{\rm eq,A})$  for donor emission and acceptor absorption, respectively, as well as a convolution kernel,  $K_{\mu\nu}(\omega_1 - \omega_2)$ , which describes the line shape of common vibrational modes shared by the two moieties:

$$L_{\mu\nu}^{\rm D,em}(\omega_1 - \omega_{\mu 0}^{\rm eq,D}) = 2\pi\hbar \sum_{m_1,n_1} f(\varepsilon_{m_1}^{\rm (e_D\mu)}) \left| \langle \Theta_{m_1}^{\rm (e_D\mu)} | \Theta_{n_1}^{\rm (g_D\nu)} \rangle \right|^2 \delta(\varepsilon_{n_1}^{\rm (g_D\nu)} - \varepsilon_{m_1}^{\rm (e_D\mu)} + \hbar(\omega_1 - \omega_{\mu 0}^{\rm eq,D}))$$
(24a)

$$L_{\mu\nu}^{\text{A,abs}}(\omega_{2} - \omega_{0\nu}^{\text{eq,A}}) = 2\pi\hbar \sum_{m_{2},n_{2}} f(\varepsilon_{m_{2}}^{(\text{gA}\mu)}) \left| \langle \Theta_{m_{2}}^{(\text{gA}\mu)} | \Theta_{n_{2}}^{(\text{e_{A}}\nu)} \rangle \right|^{2} \delta(\varepsilon_{n_{2}}^{(\text{e_{A}}\nu)} - \varepsilon_{m_{2}}^{(\text{gA}\mu)} - \hbar(\omega_{2} - \omega_{0\nu}^{\text{eq,A}}))$$
(24b)

$$K_{\mu\nu}(\omega_1 - \omega_2) = 2\pi\hbar \sum_{m_3, n_3} f(\varepsilon_{m_3}^{(I\mu)}) \left| \langle \Theta_{m_3}^{(I\mu)} | \Theta_{n_3}^{(II\nu)} \rangle \right|^2 \delta(\varepsilon_{n_3}^{(II\nu)} - \varepsilon_{m_3}^{(I\mu)} - \hbar(\omega_1 - \omega_2))$$
 (24c)

Substituting these line shape functions and the convolution kernel back into Eq. (15), we have the following expression for the PCEnT rate constant:

$$k_{\text{PCEnT}} = \frac{1}{4\pi^2 \hbar^2} \sum_{\mu,\nu} P_{\text{I}\mu} |V_{\mu\nu}|^2 \iint d\omega_1 d\omega_2 L_{\mu\nu}^{\text{D,em}} (\omega_1 - \omega_{\mu 0}^{\text{eq,D}}) K_{\mu\nu} (\omega_1 - \omega_2) L_{\mu\nu}^{\text{A,abs}} (\omega_2 - \omega_{0\nu}^{\text{eq,A}})$$
(25)

The total PCEnT rate constant is given by a summation of nonadiabatic transitions between all possible combinations of reactant and product vibronic states. The contribution of each pair of reactant and product vibronic states is proportional to the spectral convolution integral, which is a double integral of the donor emission and acceptor absorption spectra convoluted by the kernel  $K_{\mu\nu}(\omega_1 - \omega_2)$ . The convolution kernel arises from the common vibrational modes shared by the donor and acceptor moieties.

For intermolecular PCEnT, there are no common vibrational modes. In this case,

$$K_{\mu\nu}(\omega_1 - \omega_2) = 2\pi\delta(\omega_1 - \omega_2);$$
 for intermolecular PCEnT (26)

As a result, the spectral convolution integral reverts to a Förster-type spectral overlap integral, and Eq. (25) becomes

$$k_{\text{PCEnT}}^{\text{inter}} = \frac{1}{2\pi\hbar^2} \sum_{\mu,\nu} P_{\text{I}\mu} |V_{\mu\nu}|^2 \int d\omega L_{\mu\nu}^{\text{D,em}} (\omega - \omega_{\mu 0}^{\text{eq,D}}) L_{\mu\nu}^{\text{A,abs}} (\omega - \omega_{0\nu}^{\text{eq,A}})$$
(27)

The line shape functions,  $L_{\mu\nu}^{\rm D,em}(\omega-\omega_{\mu0}^{\rm eq,D})$  and  $L_{\mu\nu}^{\rm A,abs}(\omega-\omega_{0\nu}^{\rm eq,A})$ , depend on the reactant and product vibronic states  $\mu$  and  $\nu$  in two different ways. First, the arguments of the functions,  $\omega-\omega_{\mu0}^{\rm eq,D}$  and  $\omega-\omega_{0\nu}^{\rm eq,A}$ , strongly depend on  $\mu$  and  $\nu$ . Different  $\mu$  and  $\nu$  values will shift these line shape functions along the  $\omega$  axis. Second, the functional forms themselves depend on  $\mu$  and  $\nu$ . This dependence arises because the wave functions and energies of the bath,  $\Theta_m^{(j\mu)}(q)$  and  $\varepsilon_m^{(j\mu)}$ , are determined by the vibronic potential energy surface, which depends on the proton vibrational states (see Eqs. (9)–(10)). We assume that the shape of the vibronic potential energy surface is solely determined by the electronic state, and therefore the proton vibrational states just shift the energy. In this case, the functional forms of  $L_{\mu\nu}^{\rm D,em}$  and  $L_{\mu\nu}^{\rm A,abs}$ , as well as  $K_{\mu\nu}$ , are the same for every  $\mu$  and  $\nu$  pair:

$$L_{\mu\nu}^{\rm D,em}(\omega - \omega_{\mu 0}^{\rm eq,D}) = L_{\rm D,em}(\omega - \omega_{\mu 0}^{\rm eq,D})$$
 (28a)

$$L_{\mu\nu}^{\text{A,abs}}(\omega - \omega_{0\nu}^{\text{eq,A}}) = L_{\text{A,abs}}(\omega - \omega_{0\nu}^{\text{eq,A}})$$
(28b)

$$K_{\mu\nu}(\omega_1 - \omega_2) = K(\omega_1 - \omega_2) \tag{28c}$$

A similar assumption was also made in our derivation of analytical PCET rate constant expressions, where we assumed that the reactant and product vibronic free energy surfaces along the collective solvent coordinates have the same shape for all proton vibrational states (i.e., two sets of stacked paraboloids), and therefore the reorganization energy is the same for each pair of vibronic states.<sup>49,51</sup> This assumption is not strictly valid, but the resulting PCET theory has been able to describe a wide range of experimental systems.<sup>51</sup> With this assumption, Eq. (25) becomes

$$k_{\text{PCEnT}} = \frac{1}{4\pi^2 \hbar^2} \sum_{\mu,\nu} P_{\text{I}\mu} |V_{\mu\nu}|^2 \iint d\omega_1 d\omega_2 L_{\text{D,em}} (\omega_1 - \omega_{\mu 0}^{\text{eq,D}}) K(\omega_1 - \omega_2) L_{\text{A,abs}} (\omega_2 - \omega_{0\nu}^{\text{eq,A}}) \quad (29)$$

This is the general expression for the nonadiabatic PCEnT rate constant. Several specific cases of this general expression will be given in Sections III and IV below.

Similar to proton transfer and PCET, the PCEnT rate constant will depend on the proton donor-acceptor distance.<sup>50,57–59</sup> The proton donor-acceptor motion can be included in this theory by thermally averaging the rate constant over this distance. The thermally averaged PCEnT rate

constant can be expressed as

$$k_{\text{PCEnT}}^{\text{therm-avg}} = \int dR_{\text{PT}} k_{\text{PCEnT}}(R_{\text{PT}}) P(R_{\text{PT}})$$
 (30)

where  $P(R_{PT})$  is the probability distribution function for the proton donor-acceptor distance  $R_{PT}$ . Here  $k_{PCEnT}(R_{PT})$  is obtained from the general rate constant expression in Eq. (29), or alternatively one of the more specific expressions given below, at a series of different values of  $R_{PT}$ . In some cases, alternative treatments of the proton donor-acceptor motion may be warranted (i.e., when this motion has high frequency or is strongly coupled to the solvent).<sup>57–59</sup>

#### C Vibronic Coupling

The vibronic coupling for PCEnT is given by

$$V_{\mu\nu} = \left\langle \psi_{\mathrm{I}}(\boldsymbol{r}_{\mathrm{e}}; \boldsymbol{r}_{\mathrm{p}}, \boldsymbol{q}^{*}) \chi_{\mu}^{(\mathrm{I})}(\boldsymbol{r}_{\mathrm{p}}; \boldsymbol{q}^{*}) \middle| \hat{H}_{\mathrm{el}} + \hat{T}_{\mathrm{p}} \middle| \psi_{\mathrm{II}}(\boldsymbol{r}_{\mathrm{e}}; \boldsymbol{r}_{\mathrm{p}}, \boldsymbol{q}^{*}) \chi_{\nu}^{(\mathrm{II})}(\boldsymbol{r}_{\mathrm{p}}; \boldsymbol{q}^{*}) \right\rangle$$

$$\approx \left\langle \chi_{\mu}^{(\mathrm{I})}(\boldsymbol{r}_{\mathrm{p}}; \boldsymbol{q}^{*}) \middle| V_{\mathrm{el}}(\boldsymbol{r}_{\mathrm{p}}) \middle| \chi_{\nu}^{(\mathrm{II})}(\boldsymbol{r}_{\mathrm{p}}; \boldsymbol{q}^{*}) \right\rangle$$
(31)

where  $V_{\rm el}(\boldsymbol{r}_{\rm p}) = \langle \psi_{\rm I}(\boldsymbol{r}_{\rm e}; \boldsymbol{r}_{\rm p}, \boldsymbol{q}^*) | \hat{H}_{\rm el} | \psi_{\rm II}(\boldsymbol{r}_{\rm e}; \boldsymbol{r}_{\rm p}, \boldsymbol{q}^*) \rangle$  is the electronic coupling, and  $\boldsymbol{q}^*$  denotes a specified set of fixed bath coordinates, which is typically chosen to be the crossing point of the two diabatic vibronic states. Note that the second equality is an approximation because the first- and second-derivative coupling terms related to the derivatives of the electronic wave functions for the diabatic electronic states I and II with respect to the proton coordinate are assumed to be zero. Moreover, since we have applied the Condon approximation for the bath coordinates,  $V_{\rm el}$  is independent of  $\boldsymbol{q}$ , but it could depend on the position of the transferring proton. In this case,  $V_{\rm el}$  is calculated as a function of the proton position, and the matrix element in Eq. (31) is computed numerically. If we also apply the Condon approximation for the proton, assuming that  $V_{\rm el}$  is independent of the proton coordinate, the vibronic coupling becomes the product of the electronic coupling and the overlap integral between the reactant and product proton vibrational wave functions:

$$V_{\mu\nu} = V_{\rm el} S_{\mu\nu} \tag{32}$$

where  $S_{\mu\nu} = \langle \chi_{\mu}^{(\rm I)} | \chi_{\nu}^{(\rm II)} \rangle$ . We have shown that this Condon approximation for the proton is satisfied for many PCET systems.<sup>61</sup> Morever, this expression corresponds to electronically nonadiabatic proton transfer within a general semiclassical formulation for the vibronic coupling derived for PCET.<sup>60–62</sup> Note that the vibronic coupling can be much less than the thermal energy even for a relatively large electronic coupling if the overlap  $S_{\mu\nu}$  is sufficiently small.

The quantity  $V_{\rm el}$  in PCEnT theory is the same as that in Förster-Dexter theory for conventional EnT. Generally,  $V_{\rm el}$  includes contributions from both the Coulomb and exchange interactions between the electrons. For singlet-singlet PCEnT, when the separation between the donor and acceptor moieties is large, the exchange interaction can be ignored due to the negligible electronic wave function overlap. Furthermore, a dipole-dipole approximation can be used to model the Coulomb interaction, leading to the famous dipole-dipole coupling term in Förster theory:<sup>22</sup>

$$V_{\rm el}^{\rm F\ddot{o}rster} pprox \kappa \frac{|d_{\rm D}||d_{\rm A}|}{R^3}$$
 (33)

where  $d_D$  and  $d_A$  are the transition dipole moments for the donor moiety and acceptor moiety, respectively. This expression assumes that the electronic wave functions and the transition dipole moments are real quantities. In addition,  $\kappa$  is the orientational factor, defined as

$$\kappa = e_{d_D} \cdot e_{d_A} - 3(e_{d_D} \cdot e_R)(e_{d_A} \cdot e_R) \tag{34}$$

where  $e_v$  denotes the unit vector along the direction of vector v, and R is the vector connecting the donor and acceptor moieties. If the Condon approximation were not made for the proton,  $V_{\rm el}$  would have exactly the same expression, but the transition dipoles and the orientational factor would depend on the proton position, potentially leading to additional complications.

The dipole-dipole approximation is valid when the intermolecular distance R is larger than the size of both parts, typically beyond 10 Å. $^{26,63}$  For a smaller donor-acceptor separation, higher-order multipole terms as well as the exchange coupling may also need to be included. However, the dipole-dipole coupling will still be the dominant contribution even when the intermolecular distance is smaller than 10 Å. $^{63-65}$  One exception is triplet-triplet PCEnT, where the Coulomb interaction vanishes due to the orthogonality of electrons with different spin. This case leads to Dexter-type exchange coupling: $^{27}$ 

$$V_{\rm el}^{\rm Dexter} \propto e^{-\frac{R}{R_{\rm mol}}}$$
 (35)

which decreases exponentially with R. Here  $R_{\text{mol}}$  is a parameter that characterizes the size of the donor and acceptor moieties. Several methods have been developed to calculate  $V_{\text{el}}$  for triplet-triplet EnT,<sup>66</sup> which could also be adopted for PCEnT.

# III Numerical Illustrations

#### A General Considerations

The physical quantities needed for the practical application of Eq. (29) are listed in Table 1. They can be grouped into three classes. The first class is the electronic properties of the PCEnT system, including the transition dipole moments of the donor and acceptor moieties,  $d_D$  and  $d_A$ , the transition frequencies (including the proton vibrational zero-point energies),  $\omega_{00}^{\text{eq,D/A}}$  and  $\omega_{00}^{\perp,D/A}$ , and the potential energy surfaces for the proton,  $E_{\rm I}(r_{\rm p})$  and  $E_{\rm II}(r_{\rm p})$ , computed for a specified set of bath coordinates. In practice, typically the proton potential energy surfaces are assumed to be one-dimensional proton potential energy curves with shapes that are independent of the bath coordinates. Although different bath coordinates will shift the energies of these proton potentials, such shifts are already contained in  $\omega_{00}^{\rm eq,D/A}$  and  $\omega_{00}^{\perp,D/A}$ . The transition dipole moments  $d_D$  and  $d_A$  can be used to calculate the electronic coupling  $V_{\rm el}$  using Eq. (33), which is a good approximation for singlet-singlet PCEnT processes. All these quantities can be calculated using conventional electronic structure methods such as time-dependent density functional theory (TDDFT) and correlated wave function methods.

The second class of quantities includes the proton vibrational energy levels,  $\varepsilon_{\mu}^{(I)}$  and  $\varepsilon_{\nu}^{(II)}$ , and wave functions,  $\chi_{\mu}^{(I)}$  and  $\chi_{\nu}^{(II)}$ . They can be calculated numerically by solving the Schrödinger equation for the proton moving on the potential energy surfaces  $E_{\rm I}(\mathbf{r}_{\rm p})$  and  $E_{\rm II}(\mathbf{r}_{\rm p})$  using the Fourier grid Hamiltonian (FGH) method.<sup>67</sup> These quantities in turn determine the Boltzmann populations of the reactant vibronic states,  $P_{\rm I}$ , the overlap integrals  $S_{\mu\nu}$ , and the vibronic transition frequencies,

$$\omega_{\mu 0}^{\text{eq,D}} = \omega_{00}^{\text{eq,D}} + \frac{\varepsilon_{\mu}^{(I)} - \varepsilon_{0}^{(I)}}{\hbar}$$
(36a)

$$\omega_{0\nu}^{\text{eq,A}} = \omega_{00}^{\text{eq,A}} + \frac{\varepsilon_{\nu}^{(\text{II})} - \varepsilon_{0}^{(\text{II})}}{\hbar}$$
(36b)

$$\omega_{\mu 0}^{\perp, D} = \omega_{00}^{\perp, D} + \frac{\varepsilon_{\mu}^{(I)} - \varepsilon_{0}^{(I)}}{\hbar}$$
 (36c)

$$\omega_{0\nu}^{\perp,A} = \omega_{00}^{\perp,A} + \frac{\varepsilon_{\nu}^{(II)} - \varepsilon_{0}^{(II)}}{\hbar}$$
(36d)

For the third class of quantities, we need to know the functional forms of the line shape functions,  $L_{\rm D,em}(\omega)$  and  $L_{\rm A,abs}(\omega)$ , as well as the convolution kernel  $K(\omega)$ . These functions can have arbitrary forms as long as they are properly normalized:

$$\int_{-\infty}^{\infty} L_{\mathrm{D,em}}(\omega) \, \mathrm{d}\omega = \int_{-\infty}^{\infty} L_{\mathrm{A,abs}}(\omega) \, \mathrm{d}\omega = \int_{-\infty}^{\infty} K(\omega) \, \mathrm{d}\omega = 2\pi$$
 (37)

Table 1: Physical Quantities Needed to Calculate PCEnT Rate Constant

Class	Quantities	Calculation
Electronic structure	$oldsymbol{d}_{\mathrm{D}},oldsymbol{d}_{\mathrm{A}},\ \omega_{00}^{\mathrm{eq,D/A}},\omega_{00}^{\perp,\mathrm{D/A}},^{a}$	Conventional electronic structure methods such as TDDFT
Proton states	$rac{E_{ m I}(oldsymbol{r}_{ m p}),E_{ m II}(oldsymbol{r}_{ m p})}{arepsilon_{\mu}^{({ m I})},arepsilon_{ u}^{({ m II})},b}$	Solve 1D Schrödinger equation for proton using FGH method
Line shape functions	$L_{\mathrm{D,em}}(\omega), L_{\mathrm{A,abs}}(\omega), \ K(\omega)$	Model as Gaussian or Lorentzian line shapes; Extract from experimental spectra; Calculate vibrationally resolved electronic spectra

<sup>&</sup>lt;sup>a</sup> These frequencies include the proton vibrational zero-point energies.

The simplest approach is to model these functions as Gaussian or Lorentzian line shapes. A properly normalized Gaussian line shape function is given by

$$L(\omega - \omega^{\perp}; s) = \frac{2\pi\hbar}{\sqrt{2\pi s k_{\rm B} T}} \exp\left(-\frac{\hbar^2 (\omega - \omega^{\perp})^2}{2s k_{\rm B} T}\right)$$
(38)

where s is the Stokes shift in units of energy. For harmonic potential energy surfaces,  $s = 2\lambda$ , where  $\lambda$  is the reorganization energy for the bath, as defined in Eq. (22). The relationship between  $\omega^{\perp}$  and  $\omega^{\text{eq}}$  is given in the Supplementary Material. A properly normalized Lorentzian line shape function is

$$L(\omega - \omega^{\text{eq}}; \gamma) = \frac{2\gamma}{(\omega - \omega^{\text{eq}})^2 + \gamma^2}$$
(39)

where  $\gamma$  is the parameter determining the spectral width. Note that the Gaussian line shape is centered at the vertical transition frequency, whereas the Lorentzian line shape is centered at the equilibrium transition frequency.<sup>25</sup> See the Supplementary Material for derivations of the Gaussian line shape functions.

The advantage of using Gaussian and Lorentzian line shapes is that the spectral convolution integral can be calculated analytically. On the other hand, these simple models fail to capture any details of the actual spectra, especially the modulation of the line shape by high-frequency

 $<sup>^{</sup>b}$   $\varepsilon_{\mu}^{(I)}$  and  $\varepsilon_{\nu}^{(II)}$  are the proton vibrational energies relative to the minimum of the corresponding proton potential.

vibrational modes (see Supplementary Material). To obtain a better description of these line shape functions, the vibrationally resolved electronic spectra can be calculated for the donor and acceptor moieties.  $^{68,69}$  Similar to Förster theory, for intermolecular PCEnT, the spectral line shapes can be obtained from the spectra of the individual molecules. For intramolecular PCEnT, the line shape functions for the donor and acceptor moieties will be the same as the line shape functions for the individual donor and acceptor molecules if the bath modes coupled to only the donor or acceptor moieties are the same as the bath modes coupled to the individual donor or acceptor molecules. This assumption is typically valid unless the common modes are strongly coupled with some modes of the donor or acceptor. If one pair of vibronic states  $|G\sigma\rangle$  and  $|I\mu\rangle$  dominates the donor emission, and one pair of vibronic states  $|G\sigma\rangle$  and  $|II\nu\rangle$  dominates the acceptor absorption, the line shape functions can be extracted from experimentally measured spectra in a straightforward manner. A more detailed discussion about the relation between the line shape functions  $L_{\rm D,em}(\omega)$  and  $L_{\rm A,abs}(\omega)$  and the experimentally measured spectra is provided in Section IV.A.

### **B** Examples

In this section, we use a model system to illustrate key features of the PCEnT process. The diabatic proton potentials,  $E_{\rm G}(r_{\rm p})$ ,  $E_{\rm I}(r_{\rm p})$ , and  $E_{\rm II}(r_{\rm p})$ , are modeled as asymmetric double-well potentials. For simplicity, we assume that  $E_{\rm G}(r_{\rm p})$  and  $E_{\rm I}(r_{\rm p})$  have the same potential energy profile and only differ by a vertical shift of the energy. Figure 3a schematically depicts these proton potentials with the transition frequencies  $\omega_{\mu 0}^{\perp, \rm D}$  and  $\omega_{0\nu}^{\perp, \rm A}$  annotated. Note that  $\omega_{\mu 0}^{\perp, \rm D}$  and  $\omega_{0\nu}^{\perp, \rm A}$  are calculated at different bath coordinates. For  $\omega_{\mu 0}^{\perp, \rm D}$ , the bath coordinate is the equilibrium position on state  $|{\rm II}\rangle$ ,  $q_{\rm eq}^{\rm (I)}$ , while for  $\omega_{0\nu}^{\perp, \rm A}$ , the bath coordinate is  $q_{\rm eq}^{\rm (G)}$  (see Eq. (22) and Figure 2). As discussed above, we have assumed that the equilibrium position of the bath coordinate is solely determined by the electronic state, and the shape of the proton potential is independent of the bath coordinate. Therefore, changing the bath coordinate just shifts the energy (see black and gray curves in Figure 3a). The line shape functions,  $L_{\rm D,em}(\omega)$  and  $L_{\rm A,abs}(\omega)$ , are modeled as Gaussian line shapes given by Eq. (38). For PCEnT, there will be two manifolds of Gaussian line shape functions centered at  $\omega_{\mu 0}^{\perp, \rm D}$  or  $\omega_{0\nu}^{\perp, \rm A}$ . Increasing  $\mu$  or  $\nu$  shifts them toward higher frequencies, as illustrated in Figure 3b. Finally, we assume that the vibronic coupling has the form given in Eq. (32). Eq. (29) can then be

rewritten using the notations introduced in Eqs. (32) and (38) as

$$k_{\text{PCEnT}} = \frac{1}{4\pi^{2}\hbar^{2}} |V_{\text{el}}|^{2} \sum_{\mu,\nu} P_{\text{I}\mu} |S_{\mu\nu}|^{2} \times \iint d\omega_{1} d\omega_{2} L_{\text{D,em}}(\omega_{1} - \omega_{\mu 0}^{\perp,D}; s_{\text{D}}) K(\omega_{1} - \omega_{2}) L_{\text{A,abs}}(\omega_{2} - \omega_{0\nu}^{\perp,A}; s_{\text{A}})$$
(40)

We investigate how the PCEnT rate constant changes with the relative magnitudes of  $\omega_{00}^{\perp,D}$  and  $\omega_{00}^{\perp,A}$  by fixing  $\omega_{00}^{\perp,D}$  and varying  $\omega_{00}^{\perp,A}$ . This is equivalent to changing the reaction free energy  $\Delta G^{\circ} = G_{\text{II}0} - G_{\text{I0}}$  of the system.  $\Delta G^{\circ}$  is related to the frequencies as (see Figure 2)

$$\Delta G^{\circ} = \hbar (\omega_{00}^{\perp, A} - \omega_{00}^{\perp, D}) - (\lambda_{00}^{D} + \lambda_{00}^{A})$$
(41)

and the reorganization energy is related to the Stokes shift in Gaussian line shapes via  $s_{\rm D}=2\lambda_{00}^{\rm D}$  and  $s_{\rm A}=2\lambda_{00}^{\rm A}$ . Note that the surfaces in Figure 2 are free energy surfaces when they are interpreted as the potential of mean force along a collective bath coordinate. The values of the parameters  $V_{\rm el}$ ,  $\omega_{00}^{\perp,\rm D}$ ,  $\omega_{00}^{\perp,\rm A}$ ,  $s_{\rm D}$ , and  $s_{\rm A}$  used in this model system are listed in Table 2. Note that we simulated a wide range of  $\omega_{00}^{\perp,\rm A}$  in this model study, corresponding to a  $\Delta G^{\circ}$  between +0.2 eV to -1.2 eV. A realistic PCEnT system may not experience such a large range of driving force.

Table 2: Parameters for the Model PCEnT System

Parameter	Value
$V_{ m el}$	$1~\rm kcal/mol$
$\hbar\omega_{00}^{\perp,\mathrm{D}} \ \hbar\omega_{00}^{\perp,\mathrm{A}}$	$2.675~\mathrm{eV}$
$\hbar\omega_{00}^{\perp,\mathrm{A}}$	1.975 - 3.375  eV
$s_{ m D}$	0.5  eV
$s_{ m A}$	0.5 eV

We first study an intermolecular PCEnT process, where the convolution kernel is given by Eq. (26). Figure 4a depicts the calculated proton vibrational energy levels and wave functions for both the reactant ( $\mu = 0$ ) and the product ( $\nu = 0 - 5$ ). The reactant and product correspond to the energy localized on the donor (D, state  $|I\rangle$ ) or acceptor (A, state  $|II\rangle$ ), respectively. For simplicity, the reactant and product proton potentials,  $E_{\rm I}$  and  $E_{\rm II}$  defined in Eq. 7, are mirror images of each other about the point  $r_{\rm p} = 0$  for this model system (see Supplementary Material). The reactant and product states will thus have identical proton vibrational energy levels, and excited proton

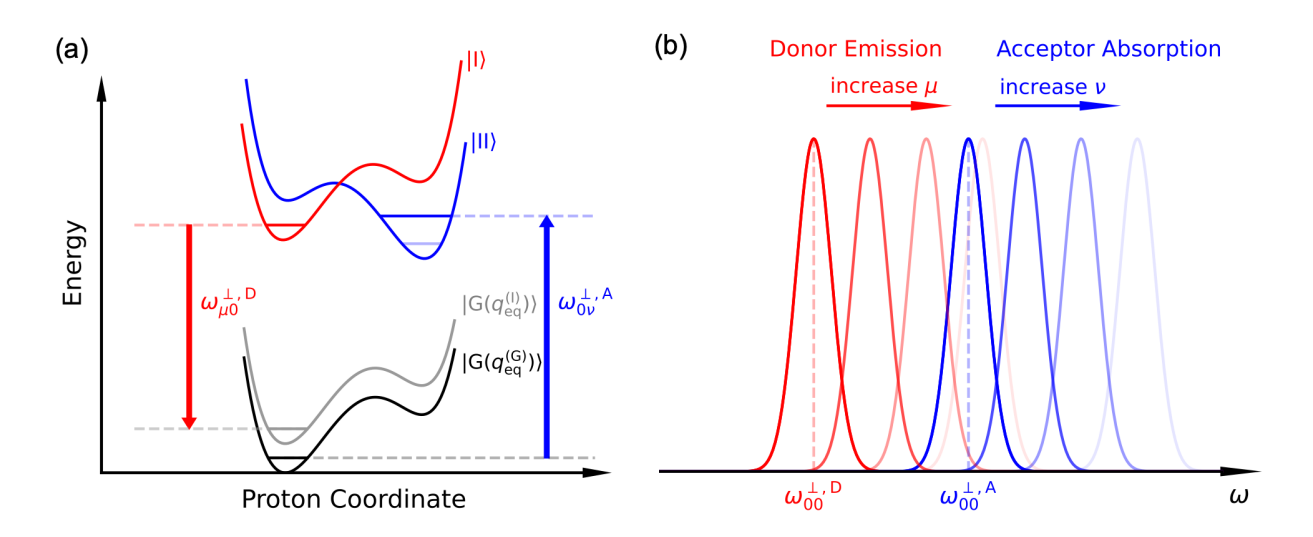


Figure 3: (a) Schematic illustration of the asymmetric double-well proton potentials used in the model, with the transition frequencies  $\omega_{\mu 0}^{\perp, \mathrm{D}}$  and  $\omega_{0\nu}^{\perp, \mathrm{A}}$  ( $\mu = 0, \nu = 1$ ) indicated. The proton potentials for states  $|\mathrm{I}\rangle$  (red) and  $|\mathrm{G}(\boldsymbol{q}_{\mathrm{eq}}^{(\mathrm{I})})\rangle$  (gray) are plotted at the equilibrium bath coordinate for state  $|\mathrm{I}\rangle$ , and the proton potentials for states  $|\mathrm{G}(\boldsymbol{q}_{\mathrm{eq}}^{(\mathrm{G})})\rangle$  (black) and  $|\mathrm{II}\rangle$  (blue) are plotted at the equilibrium bath coordinate for state  $|\mathrm{G}\rangle$ . (b) Schematic illustration of the two manifolds of Gaussian line shape functions  $L_{\mathrm{D,em}}(\omega - \omega_{\mu 0}^{\perp,\mathrm{D}}, s_{\mathrm{D}})$  and  $L_{\mathrm{A,abs}}(\omega - \omega_{0\nu}^{\perp,\mathrm{A}}, s_{\mathrm{A}})$  for donor emission and acceptor absorption.

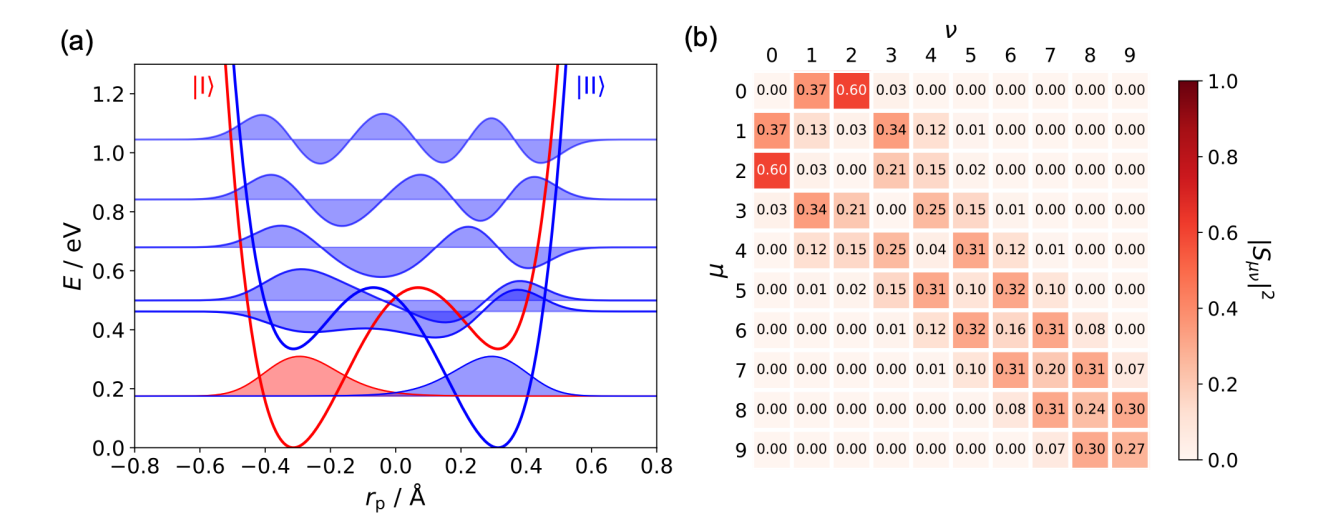


Figure 4: (a) Model reactant (red) and product (blue) proton potentials and the associated proton vibrational energy levels and wave functions. The minimum energy is set to zero for each proton potential. (b) Square of the proton vibrational overlap integral  $|S_{\mu\nu}|^2$  between the first 10 reactant and product proton vibrational states. Darker color indicates larger overlap.

vibrational wave functions of the reactant and product will also be mirror images of each other. For this double-well potential, the first and second excited vibrational states are nearly degenerate and are 0.29 eV and 0.32 eV higher in energy than the ground vibrational state. For the reactant, the Boltzmann population  $P_{I\mu}$  of the reactant vibronic states  $\mu = 1$  and  $\mu = 2$  are only  $1.4 \times 10^{-5}$  and  $3.3 \times 10^{-6}$ , respectively, at 298 K. Despite the low population, however, these excited reactant vibronic states can still contribute significantly to the overall PCEnT rate constant, as discussed below. The square of the overlap integral between the reactant and product proton vibrational wave functions,  $|S_{\mu\nu}|^2$ , is shown in Figure 4b. The maximum overlap was found for two pairs of vibronic states,  $(\mu, \nu) = (0, 2)$  and (2, 0).

The calculated spectral convolution integrals  $I_{\mu\nu}$  between vibronic states  $\mu$  and  $\nu$  are plotted for  $\hbar\omega_{00}^{\perp,A} = 3.175$  eV and  $\hbar\omega_{00}^{\perp,A} = 2.175$  eV in Figures 5a and 5c, respectively. The quantity  $I_{\mu\nu}$  is defined as the double integral appearing in Eq. (40) and is given by

$$I_{\mu\nu} = \iint d\omega_1 d\omega_2 L_{D,em}(\omega_1 - \omega_{\mu 0}^{\perp,D}; s_D) K(\omega_1 - \omega_2) L_{A,abs}(\omega_2 - \omega_{0\nu}^{\perp,A}; s_A)$$
(42)

For the case of intermolecular PCEnT,  $K(\omega_1 - \omega_2)$  becomes a delta function (Eq. 26), and the spectral convolution integral is reduced to a Förster-type spectral overlap integral. However, the spectra correspond to transitions between vibronic states instead of electronic states. As illustrated

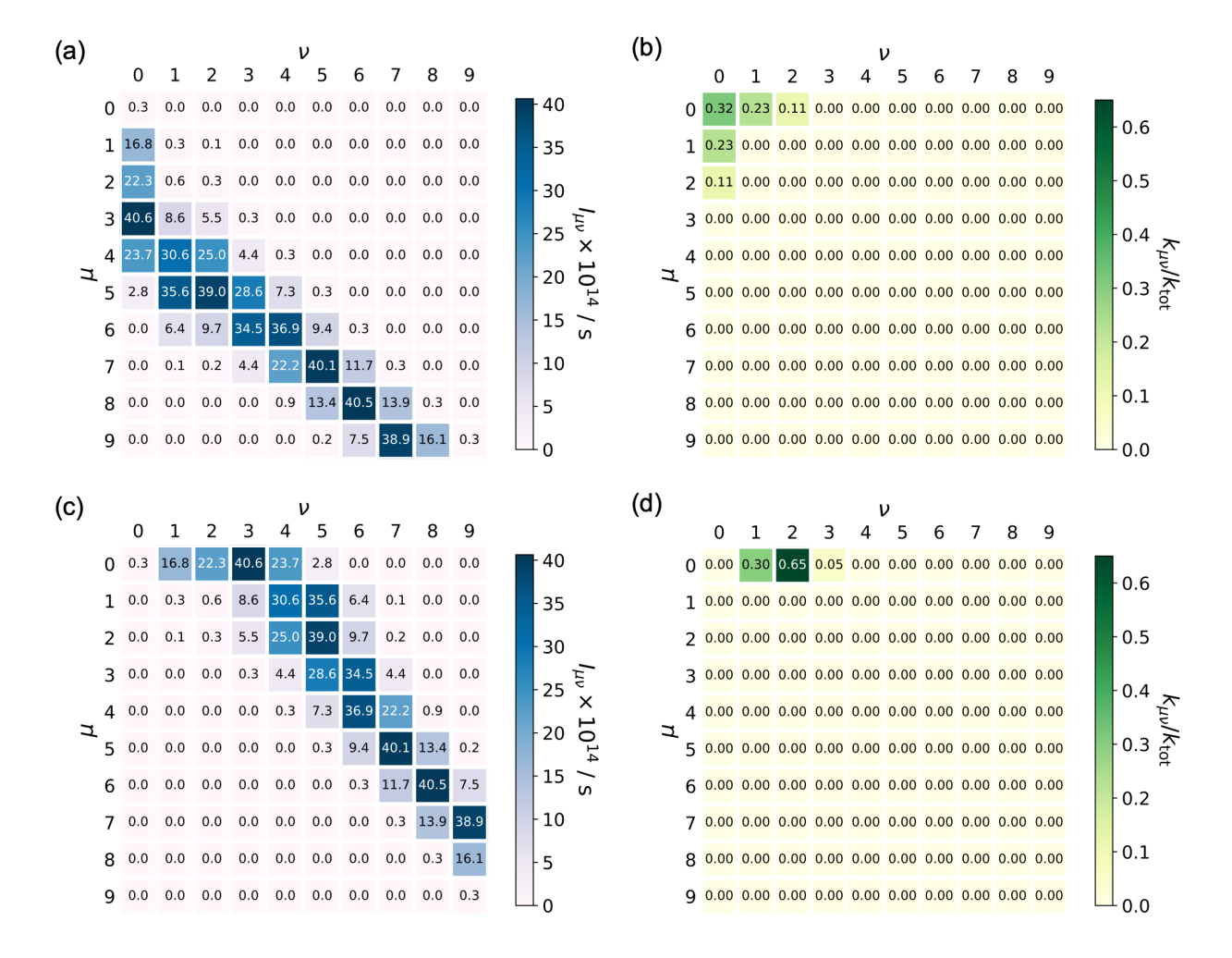


Figure 5: (a)(c) Spectral convolution integral  $I_{\mu\nu}$  between the first 10 reactant and product vibronic states. (b)(d) Percentage contribution of each pair of reactant and product vibronic states to the total PCEnT rate constant. In this model,  $\hbar\omega_{00}^{\perp,D} = 2.675 \,\mathrm{eV}$ . In (a) and (b),  $\hbar\omega_{00}^{\perp,A} = 3.175 \,\mathrm{eV}$ , corresponding to  $\Delta G^{\circ} = 0.0 \,\mathrm{eV}$ . Because  $\omega_{00}^{\perp,A} > \omega_{00}^{\perp,D}$ , higher  $\mu$  and lower  $\nu$  states have the largest  $I_{\mu\nu}$ . In (c) and (d),  $\hbar\omega_{00}^{\perp,A} = 2.175 \,\mathrm{eV}$ , corresponding to  $\Delta G^{\circ} = -1.0 \,\mathrm{eV}$ . Because  $\omega_{00}^{\perp,A} < \omega_{00}^{\perp,D}$ , lower  $\mu$  and higher  $\nu$  states have the largest  $I_{\mu\nu}$ . Other parameters used for this figure are given in Table 2, and the convolution kernel is given by Eq. (26), corresponding to intermolecular PCEnT.

in Figure 3b, both manifolds of Gaussian line shape functions shift toward higher frequencies with increasing  $\mu$  or  $\nu$ . The spectral overlap integral reaches its maximum when  $\omega_{0\nu}^{\perp,A} \approx \omega_{\mu 0}^{\perp,D}$ . Figure 3b also shows that when  $\omega_{00}^{\perp,A} > \omega_{00}^{\perp,D}$ , the transitions from higher  $\mu$  states to lower  $\nu$  states will have larger spectral overlap, whereas when  $\omega_{00}^{\perp,A} < \omega_{00}^{\perp,D}$ , the transitions from lower  $\mu$  states to higher  $\nu$  states will have larger spectral overlap. This trend is indeed observed in our model system, as shown in Figures 5a and 5c.

The nonadiabatic rate constant between a pair of vibronic states  $\mu$  and  $\nu$  is defined as

$$k_{\mu\nu} = \frac{1}{4\pi^2 \hbar^2} |V_{\rm el}|^2 P_{\rm I}_{\mu} |S_{\mu\nu}|^2 I_{\mu\nu}$$
 (43)

and the percentage contribution of an individual pair of reactant and product vibronic states to the total PCEnT rate constant is given by

$$\% \text{ Contrib.} = \frac{k_{\mu\nu}}{k_{\text{tot}}} \tag{44}$$

where  $k_{\text{tot}} = k_{\text{PCEnT}} = \sum_{\mu,\nu} k_{\mu\nu}$ . The contributions of each pair of vibronic states to the total PCEnT rate constant with  $\hbar\omega_{00}^{\perp,A}=3.175$  eV and  $\hbar\omega_{00}^{\perp,A}=2.175$  eV cases are shown in Figures 5b and 5d, respectively. These contributions are determined by a balance among  $P_{I\mu}$ ,  $|S_{\mu\nu}|^2$ , and  $I_{\mu\nu}$ . When  $\hbar\omega_{00}^{\perp,A} = 3.175 \text{ eV} > \hbar\omega_{00}^{\perp,D}$ , only the following five  $(\mu,\nu)$  pairs of vibronic states contribute to the total PCEnT rate constant: (0,0), (0,1), (0,2), (1,0), and (2,0). Each pair has comparable contributions. The transitions from excited reactant vibronic states to the ground product vibronic state, (1,0) and (2,0), have significantly larger spectral convolution integrals  $I_{\mu\nu}$  than the other three transitions by 2 to 6 orders of magnitude (Figure 5a and Table S3). The overlap between the proton vibrational wave functions is also sizable for these two pairs of states. Therefore, they have significant contributions to the overall PCEnT rate constant despite small reactant vibronic state Boltzmann populations  $P_{I\mu}$ . On the other hand, the transitions from the ground reactant vibronic state to the ground and excited product vibronic states, (0,0), (0,1), and (0,2), have a large reactant vibronic state Boltzmann population, but the overlap between the proton vibrational wave functions is very small for the pair (0,0), and the spectral convolution integral is extremely small for pairs (0,1) and (0,2). A balance of all these effects leads to comparable contributions of the five pairs of vibronic states to the total PCEnT rate constant, which is  $4.2 \times 10^8 \, \mathrm{s}^{-1}$ . The numerical values of  $P_{I\mu}$ ,  $|S_{\mu\nu}|^2$ , and  $I_{\mu\nu}$  for the (0,0), (0,1), (0,2), (1,0), and (2,0) pairs are provided in Table S3.

When  $\hbar\omega_{00}^{\perp,A} = 2.175 \text{ eV} < \hbar\omega_{00}^{\perp,D}$ , only the (0,1) and (0,2) pairs of vibronic states contribute to the total PCEnT rate constant. For these two pairs, all three quantities,  $P_{\text{I}\mu}$ ,  $|S_{\mu\nu}|^2$ , and  $I_{\mu\nu}$ , are

sizable. Specifically, the (0,2) pair has 1.6-fold larger  $|S_{\mu\nu}|^2$  and 1.3-fold larger  $I_{\mu\nu}$  than the (0,1) pair. Therefore, the contribution of the (0,2) pair is about 2-fold larger than the contribution of the (0,1) pair. The relatively large values of  $P_{I\mu}$ ,  $|S_{\mu\nu}|^2$ , and  $I_{\mu\nu}$  for the two contributing pairs of vibronic states lead to a significantly larger PCEnT rate constant  $(2.3 \times 10^{13} \, \text{s}^{-1})$  compared to the previous case with  $\hbar\omega_{00}^{\perp,A} = 3.175$  eV. The numerical values of  $P_{I\mu}$ ,  $|S_{\mu\nu}|^2$ , and  $I_{\mu\nu}$  for the (0,1) and (0,2) pairs are provided in Table S3.

Figure 6a (black line) shows the total PCEnT rate constant as a function of the PCEnT driving force  $-\Delta G^{\circ}$ . This model PCEnT system exhibits an inverted region when  $-\Delta G^{\circ} > 0.8$  eV, where the rate constant decreases with increasing driving force. This type of inverted region behavior has also been observed in both  $\mathrm{EnT}^{70}$  and  $\mathrm{PCET}^{71,72}$  systems. As discussed previously for  $\mathrm{PCET},^{71,72}$ inverted region behavior can be observed when the overlap integrals  $S_{\mu\nu}$  for higher product proton vibrational states become negligible due to phase cancellation. This behavior is found mainly for asymmetric double-well potentials with relatively low barriers, corresponding to hydrogen-bonded systems. The same phenomenon can be observed for PCEnT for these types of systems, although additional complexity is introduced by the spectral convolution integral. Figure 6b (black line) shows the kinetic isotope effect (KIE), which is defined as the ratio between the PCEnT rate constant for hydrogen and deuterium, as a function of the driving force. The KIE has a non-monotonic dependence on the driving force, and an inverse KIE (< 1) is found at  $\Delta G^{\circ} \approx -1.0$  eV. Such behavior has been observed in model PCET systems with similar asymmetric double-well proton potentials.<sup>71</sup> Note that the driving force dependence of the rate constant and KIE observed for this model system may not be directly transferrable to experimental PCEnT systems. The behavior of experimentally studied systems will strongly depend on the shape of the proton potential profiles and the spectral line shape functions.

Next we examine the influence of common vibrational modes shared by the donor and acceptor moieties on the total rate constant and KIE in an intramolecular PCEnT system. We assume a Gaussian line shape for  $K(\omega_1 - \omega_2)$ :

$$K(\omega_1 - \omega_2) = \frac{2\pi\hbar}{\sqrt{2\pi s_{\text{com}} k_{\text{B}} T}} \exp\left(-\frac{(\hbar(\omega_1 - \omega_2) - s_{\text{com}}/2)^2}{2s_{\text{com}} k_{\text{B}} T}\right)$$
(45)

where  $s_{\text{com}}$  is the Stokes shift for the common modes. From a physical perspective,  $s_{\text{com}}$  characterizes the reorganization of the common modes during PCEnT, where a larger  $s_{\text{com}}$  indicates a larger change in the common mode coordinates. For this analysis,  $s_{\text{com}} = 0.2$  or 0.6 eV. The calculated total PCEnT rate constant and KIE are shown in Figure 6. The presence of common vibrational

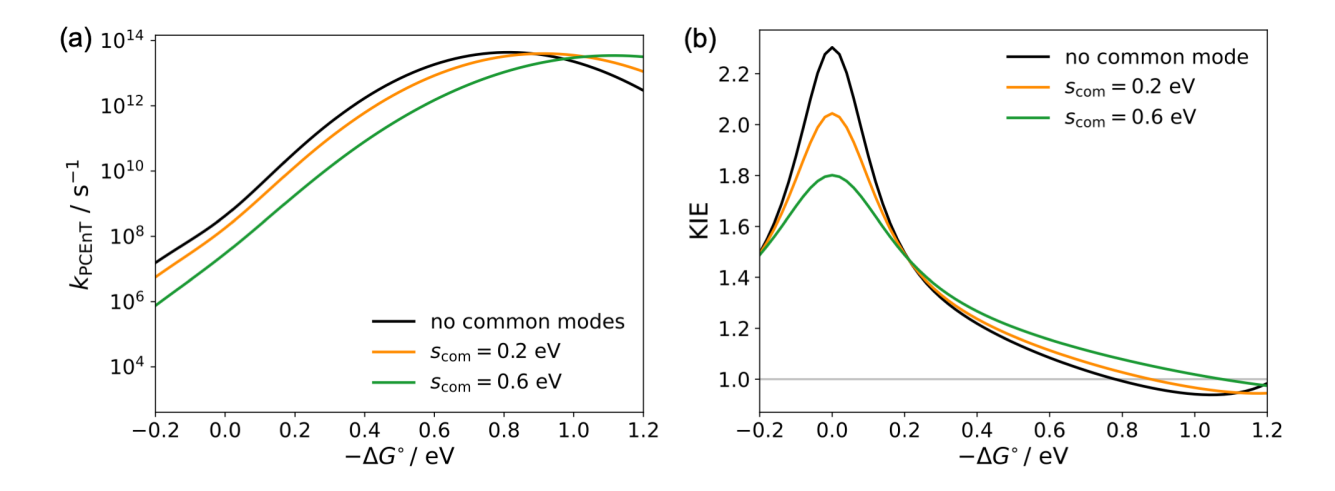


Figure 6: Driving force dependence of (a) total PCEnT rate constant and (b) KIE for a model system. The results for intermolecular PCEnT with no common modes are shown in black. The results for intramolecular PCEnT with common modes corresponding to  $s_{\text{com}} = 0.2 \text{ eV}$  and  $s_{\text{com}} = 0.6 \text{ eV}$  are shown in orange and green, respectively.

modes shifts the maximum of the  $\log k$  vs.  $-\Delta G^{\circ}$  curve to the right, and larger  $s_{\rm com}$  leads to a larger shift. At lower driving force, the common modes slow down PCEnT, while at larger driving force, the common modes speed up PCEnT. The non-monotonic change of the KIE as a function of  $-\Delta G^{\circ}$  remains the same with the presence of common modes, but the peak value of the KIE becomes smaller. Both effects arise because the convolution with  $K(\omega_1 - \omega_2)$  changes the spectral convolution integral  $I_{\mu\nu}$ .

For this model system, when  $\omega_{0\nu}^{\perp,A} < \omega_{\mu 0}^{\perp,D}$ , the common modes increase  $I_{\mu\nu}$ , whereas when  $\omega_{0\nu}^{\perp,A} > \omega_{\mu 0}^{\perp,D}$ , the common modes decrease  $I_{\mu\nu}$ . When  $\hbar\omega_{00}^{\perp,A} = 3.175 \text{ eV} > \hbar\omega_{00}^{\perp,D}$ , the common modes decrease  $I_{\mu\nu}$  for the pairs that contribute the most to the total PCEnT rate constant (Figures 5a and S2a) and thus slow down intramolecular PCEnT. When  $\hbar\omega_{00}^{\perp,A} = 2.175 \text{ eV} < \hbar\omega_{00}^{\perp,D}$ , the common modes increase  $I_{\mu\nu}$  for the pairs that contribute the most to the total PCEnT rate constant (Figures 5c and S2c) and therefore speed up the overall PCEnT process. The behavior of physically realistic systems will depend strongly on the shape of the proton potentials, the spectral line shape functions, and the convolution kernel. In summary, if some high-frequency vibrational modes (i.e., stretches) are shared by the donor and acceptor moieties,  $s_{\text{com}}$  can be large, and these common modes can significantly influence the PCEnT rate constant and KIE. Conversely, if only low-frequency modes (i.e., dihedral twists) are shared by the donor and acceptor moieties,  $s_{\text{com}}$  is

small, and the influence of the common modes may be negligible.

# IV Discussion

# A Connection to the Overlap of Experimentally Measured Spectra

Previous experiments on the triad system<sup>43</sup> suggested that PCEnT could occur without any detectable overlap between the donor (An) emission and acceptor (PhOH-py) absorption spectra. We emphasize that these experimentally measured spectra are not the same as the spectra  $L_{\rm D,em}(\omega - \omega_{\mu 0}^{\rm eq,D})$  and  $L_{\rm A,abs}(\omega - \omega_{0\nu}^{\rm eq,A})$  used in Eq. (29).  $L_{\rm D,em}(\omega - \omega_{\mu 0}^{\rm eq,D})$  and  $L_{\rm A,abs}(\omega - \omega_{0\nu}^{\rm eq,A})$  describe the line shape of the transition between specific vibronic states,  $|I\mu\rangle \rightarrow |G0\rangle$  and  $|G0\rangle \rightarrow |II\nu\rangle$ , but the experimentally measured spectra intrinsically include the contributions of all vibronic (i.e., proton vibrational) states. Using Fermi's golden rule formula, we can derive the following expressions for  $\tilde{L}_{\rm D,em}(\omega)$  and  $\tilde{L}_{\rm A,abs}(\omega)$ , which are the line shape functions of experimentally measured spectra:

$$\tilde{L}_{\mathrm{D,em}}(\omega) = \sum_{\mu,\sigma} P_{\mathrm{I}\mu} |S_{\mu\sigma}|^2 L_{\mathrm{D,em}}(\omega - \omega_{\mu\sigma}^{\mathrm{eq,D}})$$
(46a)

$$\tilde{L}_{A,abs}(\omega) = \sum_{\sigma,\nu} P_{G\sigma} |S_{\sigma\nu}|^2 L_{A,abs}(\omega - \omega_{\sigma\nu}^{eq,A})$$
(46b)

where  $\sigma$  denotes a proton vibrational state on the electronic ground state. Note that these expressions are not restricted to any specific line shapes, so the more general notation for line shape functions in Eq. (29) is used. The experimentally measured absorbance and fluorescence intensities are proportional to these line shape functions:<sup>28</sup>

Emission Intensity 
$$\propto \omega^3 \tilde{L}_{\rm D,em}(\omega)$$
 (47a)

Absorbance 
$$\propto \omega \tilde{L}_{A,abs}(\omega)$$
 (47b)

Eq. (46) indicates that the experimentally measured donor emission and acceptor absorption spectra are weighted sums of the line shape functions for transitions between vibronic states. The main peaks correspond to vibronic transitions that have significant  $P_{\text{I}\mu}|S_{\mu\sigma}|^2$  and  $P_{\text{G}\sigma}|S_{\sigma\nu}|^2$  weightings. For the model system with  $\hbar\omega_{00}^{\perp,\text{A}} = 3.175 \text{ eV}$ , the dominant vibronic transitions to the total line shape functions  $\tilde{L}_{\text{D,em}}(\omega)$  and  $\tilde{L}_{\text{A,abs}}(\omega)$  are  $|\text{I0}\rangle \to |\text{G0}\rangle$  for donor emission and  $|\text{G0}\rangle \to |\text{II2}\rangle$  for acceptor absorption. The spectral overlap integral between  $\tilde{L}_{\text{D,em}}(\omega)$  and  $\tilde{L}_{\text{A,abs}}(\omega)$  is

$$\int d\omega \, \tilde{L}_{D,em}(\omega) \tilde{L}_{A,abs}(\omega) = \sum_{\mu,\nu,\sigma,\sigma'} P_{I\mu} P_{G\sigma'} |S_{\mu\sigma}|^2 |S_{\sigma'\nu}|^2 \int d\omega \, L_{D,em}(\omega - \omega_{\mu\sigma}^{eq,D}) L_{A,abs}(\omega - \omega_{\sigma'\nu}^{eq,A})$$
(48)

For the model system with  $\hbar\omega_{00}^{\perp,A}=3.175\,\text{eV}$ , this integral is approximately  $\int d\omega\,\tilde{L}_{D,\text{em}}(\omega)\tilde{L}_{A,\text{abs}}(\omega)$   $\approx \int d\omega\,L_{D,\text{em}}(\omega-\omega_{00}^{\text{eq},D})L_{A,\text{abs}}(\omega-\omega_{02}^{\text{eq},A})$  when only the dominant vibronic transitions to the total line shape functions are included. The separation between the peaks of  $\tilde{L}_{D,\text{em}}(\omega)$  and  $\tilde{L}_{A,\text{abs}}(\omega)$  is 0.82 eV. As shown in Figure 7a,  $\tilde{L}_{D,\text{em}}(\omega)$  and  $\tilde{L}_{A,\text{abs}}(\omega)$  have no apparent spectral overlap.

However, our calculation shows that this model system has a fairly large PCEnT rate constant of  $4.2 \times 10^8 \,\mathrm{s^{-1}}$ . For the simplest case with no common modes and the vibronic coupling given by Eq. (32), the PCEnT rate constant is

$$k_{\text{PCEnT}} = \frac{1}{2\pi\hbar^2} |V_{\text{el}}|^2 \sum_{\mu,\nu} P_{\text{I}\mu} |S_{\mu\nu}|^2 \int d\omega \, L_{\text{D,em}}(\omega - \omega_{\mu 0}^{\text{eq,D}}) L_{\text{A,abs}}(\omega - \omega_{0\nu}^{\text{eq,A}})$$
(49)

In contrast to the experimentally measured spectra, the pairs of vibronic states that dominate the PCEnT rate constant are determined by a balance among  $P_{1\mu}$ ,  $|S_{\mu\nu}|^2$ , and  $I_{\mu\nu}$ , which is the integral over  $\omega$  in Eq. (49). Thus, the vibronic states that dominate the donor emission and acceptor absorption spectra may not be the same as the vibronic states that dominate the PCEnT rate constant. Note that the overlap  $S_{\mu\nu}$  in the donor emission and acceptor absorption spectra involves proton vibrational wave functions in an excited electronic state (donor or acceptor) and the ground electronic state, whereas the overlap in the PCEnT rate constant expression involves proton vibrational wave functions in the donor and acceptor excited electronic states. For the model system with  $\hbar\omega_{00}^{\perp,A}=3.175$  eV, the (0,0) pair dominates the PCEnT rate constant (Figure 5b). The separation between the peaks of  $L_{\rm D,em}(\omega_1-\omega_{00}^{\rm eq,D})$  and  $L_{\rm A,abs}(\omega_2-\omega_{00}^{\rm eq,A})$  is 0.5 eV, leading to more significant spectral overlap (Figure 7b) and enabling PCEnT. In summary, the pairs of vibronic states that contribute the most to the PCEnT rate constant may correspond to spectroscopically dark states. Therefore, PCEnT could occur even when there is no apparent spectral overlap between the donor emission and acceptor absorption. The optically dark states have also been proposed to play important roles in certain conventional EnT processes.<sup>26,73</sup>

As mentioned in the previous section, the line shape functions  $L(\omega)$ , which are input quantities to the PCEnT rate constant expression in Eq. (29), can be extracted from experimental spectra. The experimentally measured spectra provide  $\tilde{L}(\omega)$ , which are related to the line shapes  $L(\omega)$  that appear in the PCEnT rate constant expression through Eq. (46). In practice,  $P_{I\mu}$ ,  $P_{G\sigma}$ ,  $|S_{\mu\sigma}|^2$ , and  $|S_{\sigma\nu}|^2$  can be calculated by solving the 1D Schrödinger equation for the proton potentials using the FGH method. The resulting proton vibrational wave functions and corresponding overlap integrals in turn determine the contributions of transitions  $|I\mu\rangle \to |G\sigma\rangle$  and  $|G\sigma\rangle \to |II\nu\rangle$  to the total line shape functions  $\tilde{L}(\omega)$ . If one transition dominates, such as  $|I\mu^*\rangle \to |G\sigma^*\rangle$  and  $|G\sigma^*\rangle \to |II\nu^*\rangle$ , we

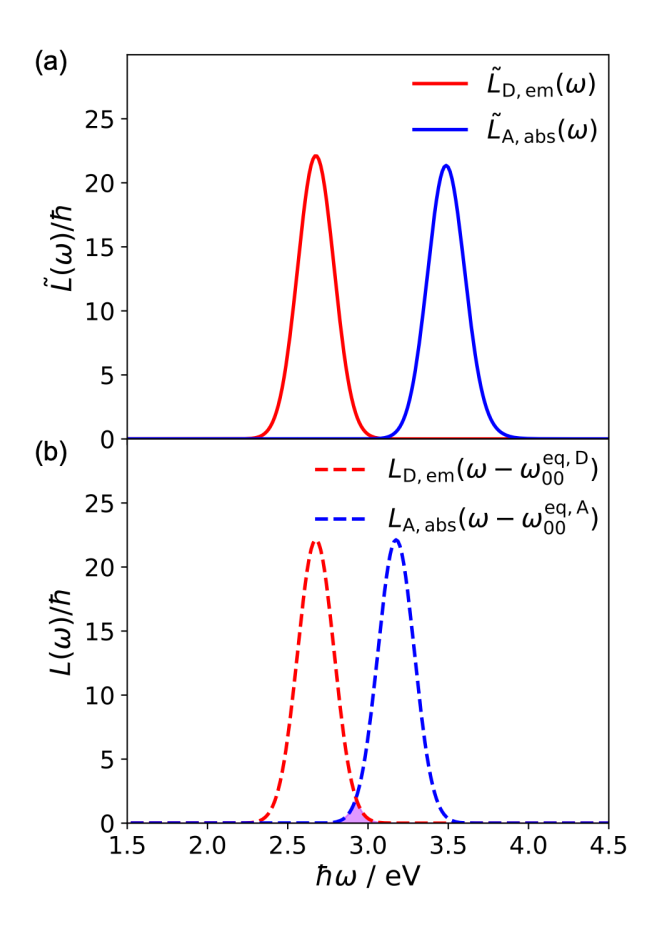


Figure 7: (a) Plots of the total donor emission and acceptor absorption line shape functions,  $\tilde{L}_{\rm D,em}(\omega)$  and  $\tilde{L}_{\rm A,abs}(\omega)$ , for the model system with  $\hbar\omega_{00}^{\perp,\rm A}=3.175$  eV. (b) Plots of the line shape functions  $L_{\rm D,em}(\omega_1-\omega_{\mu0}^{\rm eq,D})$  and  $L_{\rm A,abs}(\omega_2-\omega_{0\nu}^{\rm eq,A})$  for the (0,0) pair, which has the dominant contribution to the total PCEnT rate constant for the model system with  $\hbar\omega_{00}^{\perp,\rm A}=3.175$  eV.

can use Eq. (46) to approximate  $L_{\rm D,em}(\omega - \omega_{\mu^*\sigma^*}^{\rm eq,D})$  as  $\tilde{L}_{\rm D,em}(\omega)$  and  $L_{\rm A,abs}(\omega - \omega_{\sigma^*\nu^*}^{\rm eq,A})$  as  $\tilde{L}_{\rm A,abs}(\omega)$ . Note that  $\sigma^*$  can be different for the donor emission and acceptor absorption. Since the line shapes are assumed to be independent of the proton vibrational state, the input quantities for Eq. (29),  $L_{\rm D,em}(\omega - \omega_{\mu 0}^{\rm eq,D})$  and  $L_{\rm A,abs}(\omega - \omega_{0\nu}^{\rm eq,A})$ , can be obtained by simply changing the arguments. If there is not a single dominant transition, the line shape functions  $L(\omega)$  could be obtained from Eq. (46) numerically.

### B Connection to PCET Theory

Lastly, we compare this PCEnT theory to the PCET theory previously developed in our group.  $^{49-51}$  The two-level model Hamiltonian for PCEnT in Eq. (14) is formally the same as the model Hamiltonian for a PCET system.  $^{49}$  In the vibronically nonadiabatic limit, both the PCET and PCEnT theories are derived from Fermi's golden rule formula. These two theories are therefore closely connected to each other. If we assume Gaussian line shapes for  $L_{\rm D,em}(\omega)$ ,  $L_{\rm A,abs}(\omega)$ , and  $K(\omega_1 - \omega_2)$ , given in Eqs. (38) and (45), The spectral convolution integral can be calculated analytically, which leads to

$$k_{\text{PCEnT}}^{\text{high-T}} = \frac{2\pi}{\hbar} \sum_{\mu,\nu} P_{\text{I}\mu} |V_{\mu\nu}|^2 \frac{1}{\sqrt{4\pi\lambda_{\text{tot}}k_{\text{B}}T}} \exp\left[-\frac{(\Delta G_{\mu\nu} + \lambda_{\text{tot}})^2}{4\lambda_{\text{tot}}k_{\text{B}}T}\right]$$
(50)

where  $\Delta G_{\mu\nu} = G_{\text{II}\nu} - G_{\text{I}\mu}$ , and  $\lambda_{\text{tot}} = (s_{\text{D}} + s_{\text{A}} + s_{\text{com}})/2$ . Eq. (50) is formally the same expression as the rate constant for vibronically nonadiabatic PCET processes. In the derivation of the PCET rate constant, we used the multistate continuum model and assumed the high-temperature limit for the bath.<sup>49</sup> This high-temperature assumption is equivalent to a classical treatment of the bath degrees of freedom.<sup>55</sup> In PCEnT theory, if we model the bath modes as a set of harmonic oscillators and take the low-frequency limit, both the line shape functions and the convolution kernel become Gaussian line shapes (see Supplementary Material for full derivation). Therefore, the use of Gaussian line shape functions implies a classical assumption for the bath where  $k_{\text{B}}T \gg \hbar\omega_{\text{bath}}$ . The rate constant expressions for PCET and Eq. (50) are formally identical because they are both based on the same two-level model Hamiltonian with the same high-temperature approximation for the bath. Interestingly, in this case the PCEnT process can be viewed in terms of direction transitions between vibronic states I $\mu$  and II $\nu$ , rather than an emission and absorption process involving the ground electronic state.

Conversely, if we relax the linear response and high-temperature assumptions in the PCET theory, <sup>48,49</sup> we would arrive at an expression similar to Eq. (29). Analogous to electron transfer, <sup>25</sup> the

donor emission and acceptor absorption spectra could be interpreted in terms of spectra associated with removing an electron from the donor and adding an electron to the acceptor. Moreover, for the PCET case, the solvent bath modes may be more important.

However, we emphasize that PCET and PCEnT theories are fundamentally distinct. There are two key differences. First, Eq. (50) is only a special case to the general expression given in Eq. (29). Any arbitrary type of line shape functions, including those with structure and multiple peaks, can be used to calculate the PCEnT rate constant. Using other types of line shape functions could lead to significantly different behavior (e.g., KIE, driving force dependence, and so forth) in a PCEnT system compared to a PCET system. Second, the characters of the initial and final states are different in PCEnT and PCET. For PCEnT, the initial and final electronic states are two local excited states corresponding to electronic energy transfer. For singlet-singlet energy transfer, the electronic coupling is typically dominated by the long-range Coulomb interaction between the transition dipole moments of the donor and acceptor moieties and has an inverse sixth power dependence on the donor-acceptor separation. In contrast, the initial and final states for PCET correspond to ET states, where an electron has transferred from one moiety to another, thereby involving significant charge rearrangement. The electronic coupling is thus more short-ranged in PCET and typically depends exponentially on the donor-acceptor separation.

This analysis provides some guidelines for distinguishing between PCET and PCEnT processes. Measuring the dependence of the rate constant on the donor-acceptor distance could be one way to experimentally distinguish between photoinduced PCEnT and PCET processes, although this distinction may be less clear for Dexter-type energy transfer. Another diagnostic could be to measure the change in the molecular dipole moment to determine if electron transfer has occurred. For certain systems, such as the triads shown in Figure 1, the PCET and PCEnT process are clearly distinguishable based on the characteristics of the excited electronic states. Specifically, PCET involves electron transfer to the anthracene, resulting in a significant change in the molecular dipole moment, whereas PCEnT does not involve any charge transfer to the anthracene. For other systems, the distinction may not be as obvious.

# V Conclusion

PCEnT is a recently discovered photochemistry mechanism where the transfer of electronic excitation energies between chromophores is coupled to a proton transfer reaction. In this paper, we

derived an analytical expression for the PCEnT rate constant in the vibronically nonadiabatic limit. The final formula, Eq. (29), is expressed as a summation of the nonadiabatic transitions between all pairs of reactant and product vibronic states  $\mu$  and  $\nu$ . The contribution of each  $(\mu, \nu)$  pair to the overall PCEnT rate constant is proportional to the spectral convolution integral, which is a double integral of the donor emission and acceptor absorption spectra convoluted by the kernel  $K(\omega_1 - \omega_2)$ . The spectral line shape functions associated with emission and absorption are defined in terms of transitions between vibronic states instead of electronic states. The convolution kernel arises from the common bath modes shared by the donor and acceptor moieties, such as the solute vibrational modes associated with the bridge connecting the donor and acceptor for intramolecular PCEnT. The contribution of each  $(\mu, \nu)$  pair to the overall PCEnT rate constant is also proportional to the square of the vibronic coupling  $|V_{\mu\nu}|^2$ , which in certain limits can be calculated as a product of the electronic coupling and the overlap integral between reactant and product proton vibrational wave functions. The electronic coupling can be calculated with the same expressions as used in Förster and Dexter theories for EnT. Thus, Eq. (29) is valid for both intermolecular and intramolecular PCEnT and can be applied to both singlet-singlet and triplet-triplet PCEnT.

We illustrated the practical application of this theory for a model PCEnT system. We calculated the total PCEnT rate constant and the contribution of each  $(\mu, \nu)$  pair under two different conditions: the acceptor absorption frequency is higher or lower than the donor emission frequency. For both cases, we found significant contributions from the excited vibronic states. These contributions are determined by a subtle balance among the initial vibronic state population, the overlap between the reactant and product proton vibrational wave functions, and the spectral convolution integral between the vibronic states. We also studied the influence of the common vibrational modes on the PCEnT rate constant. Depending on the driving force and other characteristics of the system, the common modes can either slow down or speed up the process. The effect is more pronounced if there are some high-frequency modes shared by the donor and acceptor. Similar to conventional EnT and PCET, PCEnT could also exhibit an inverted region, where the rate constant decreases with increasing driving force, under certain conditions. Our analysis also suggests that PCET and PCEnT could be distinguished experimentally by measuring the dependence of the rate constant on the distance between the electron or energy donor and acceptor. Conventional EnT and PCEnT could be distinguished experimentally by measuring the KIE, although contributions from excited vibronic states may complicate this analysis.<sup>51</sup>

Lastly, we showed how PCEnT could occur even when there is no apparent overlap between the

donor emission and acceptor absorption spectra. Although the experimentally measured spectra contain contributions from all proton vibrational states, the vibronic transitions with significant overlap between proton vibrational wave functions associated with the donor or acceptor excited electronic state and the ground electronic state will dominate these spectra. In contrast, the pairs of vibronic states that dominate the PCEnT rate constant typically have significant overlap between proton vibrational wave functions associated with the excited electronic states of the donor and acceptor. Thus, the vibronic states that dominate the donor emission and acceptor absorption spectra may not be the same as the vibronic states that dominate the PCEnT rate constant. As a result, the PCEnT process could be dominated by vibronic transitions that correspond to spectroscopically dark states. The theory presented in this paper is a powerful tool for understanding the underlying physical principles of PCEnT processes and can be used to guide the design of new PCEnT systems.

# Supplementary Material

Derivations of line shape functions, construction of asymmetric double-well proton potentials, and additional numerical results.

# Acknowledgements

This work was supported by the National Science Foundation Grant No. CHE-1954348 and CHE-2415034. The authors thank Alexander V. Soudackov for helpful discussions.

# Data Availability

The data that supports the findings of this study are available within the article and its supplementary material.

# References

- <sup>1</sup>T. Förster and O. Sinanoglu, *Modern quantum chemistry* (Academic Press, New York, 1965).
- <sup>2</sup>R. Silbey, "Electronic energy transfer in molecular crystals", Ann. Rev. Phys. Chem. **27**, 203–223 (1976).
- <sup>3</sup>B. Meer, E. G. Coker, and S.-Y. S. Chen, Resonance energy transfer: theory and data (Wiley-VCH, New York, 1994).
- <sup>4</sup>G. D. Scholes, "Long-range resonance energy transfer in molecular systems", Ann. Rev. Phys. Chem. **54**, 57–87 (2003).
- <sup>5</sup>G. D. Scholes and G. R. Fleming, "On the mechanism of light harvesting in photosynthetic purple bacteria: b800 to b850 energy transfer", J. Phys. Chem. B **104**, 1854–1868 (2000).
- <sup>6</sup>T. Renger, V. May, and O. Kühn, "Ultrafast excitation energy transfer dynamics in photosynthetic pigment–protein complexes", Phys. Rep. **343**, 137–254 (2001).
- <sup>7</sup>X. Hu, T. Ritz, A. Damjanović, F. Autenrieth, and K. Schulten, "Photosynthetic apparatus of purple bacteria", Q. Rev. Biophys. **35**, 1–62 (2002).
- <sup>8</sup>R. J. Cogdell, A. Gall, and J. Köhler, "The architecture and function of the light-harvesting apparatus of purple bacteria: from single molecules to in vivo membranes", Q. Rev. Biophys. **39**, 227–324 (2006).
- <sup>9</sup>G. S. Engel, T. R. Calhoun, E. L. Read, T.-K. Ahn, T. Mančal, Y.-C. Cheng, R. E. Blankenship, and G. R. Fleming, "Evidence for wavelike energy transfer through quantum coherence in photosynthetic systems", Nature **446**, 782–786 (2007).
- <sup>10</sup>J. Ye, K. Sun, Y. Zhao, Y. Yu, C. Kong Lee, and J. Cao, "Excitonic energy transfer in light-harvesting complexes in purple bacteria", J. Chem. Phys. 136, 245104 (2012).
- <sup>11</sup>A. Buckley, M. Rahn, J. Hill, J. Cabanillas-Gonzalez, A. Fox, and D. Bradley, "Energy transfer dynamics in polyfluorene-based polymer blends", Chem. Phys. Lett. 339, 331–336 (2001).
- <sup>12</sup>S. Meskers, J. Hübner, M. Oestreich, and H. Bässler, "Time-resolved fluorescence studies and monte carlo simulations of relaxation dynamics of photoexcitations in a polyfluorene film", Chem. Phys. Lett. 339, 223–228 (2001).

- <sup>13</sup>K. M. Gaab and C. J. Bardeen, "Wavelength and temperature dependence of the femtosecond pump-probe anisotropies in the conjugated polymer meh-ppv: implications for energy-transfer dynamics", J. Phys. Chem. B 108, 4619–4626 (2004).
- $^{14}\mathrm{E.~R.}$  Bittner, "Simplifying organic complexity", Nat. Phys. 2, 591–592 (2006).
- <sup>15</sup>M. R. Wasielewski, "Energy, charge, and spin transport in molecules and self-assembled nanostructures inspired by photosynthesis", J. Org. Chem. **71**, 5051–5066 (2006).
- <sup>16</sup>M. R. Wasielewski, "Self-assembly strategies for integrating light harvesting and charge separation in artificial photosynthetic systems", Acc. Chem. Res. 42, 1910–1921 (2009).
- <sup>17</sup>L. Stryer and R. P. Haugland, "Energy transfer: a spectroscopic ruler.", Proc. Natl. Acad. Sci. 58, 719–726 (1967).
- <sup>18</sup>P. Wu and L. Brand, "Resonance energy transfer: methods and applications", Anal. Biochem. 218, 1–13 (1994).
- <sup>19</sup>C. Joo, H. Balci, Y. Ishitsuka, C. Buranachai, and T. Ha, "Advances in single-molecule fluorescence methods for molecular biology", Annu. Rev. Biochem. 77, 51–76 (2008).
- <sup>20</sup>B. Schuler and W. A. Eaton, "Protein folding studied by single-molecule fret", Curr. Opin. Struct. Biol. 18, 16–26 (2008).
- <sup>21</sup>J. I. Basham, G. K. Mor, and C. A. Grimes, "Förster resonance energy transfer in dye-sensitized solar cells", ACS Nano 4, 1253–1258 (2010).
- <sup>22</sup>T. Förster, "Zwischenmolekulare energiewanderung und fluoreszenz", Ann. Phys. **437**, 55–75 (1948).
- <sup>23</sup>D. Beljonne, C. Curutchet, G. D. Scholes, and R. J. Silbey, "Beyond förster resonance energy transfer in biological and nanoscale systems", J. Phys. Chem. B 113, 6583–6599 (2009).
- <sup>24</sup>S. Jang and Y.-C. Cheng, "Resonance energy flow dynamics of coherently delocalized excitons in biological and macromolecular systems: recent theoretical advances and open issues", Wiley Interdiscip. Rev. Comput. Mol. Sci. 3, 84–104 (2013).
- <sup>25</sup>V. May and O. Kühn, Charge and energy transfer dynamics in molecular systems (John Wiley & Sons, 2023).
- <sup>26</sup>K. F. Wong, B. Bagchi, and P. J. Rossky, "Distance and orientation dependence of excitation transfer rates in conjugated systems: beyond the förster theory", J. Phys. Chem. A 108, 5752–5763 (2004).

- <sup>27</sup>D. L. Dexter, "A theory of sensitized luminescence in solids", J. Chem. Phys. **21**, 836–850 (1953).
- <sup>28</sup>S. Jang, "Generalization of the förster resonance energy transfer theory for quantum mechanical modulation of the donor-acceptor coupling", J. Chem. Phys. **127**, 174710 (2007).
- <sup>29</sup>E. Hennebicq, D. Beljonne, C. Curutchet, G. Scholes, and R. Silbey, "Shared-mode assisted resonant energy transfer in the weak coupling regime", J. Chem. Phys. 130, 214505 (2009).
- <sup>30</sup>S. Jang, Y. Jung, and R. J. Silbey, "Nonequilibrium generalization of förster-dexter theory for excitation energy transfer", Chem. Phys. 275, 319–332 (2002).
- <sup>31</sup>C. Wang, J. Ren, and J. Cao, "Nonequilibrium energy transfer at nanoscale: a unified theory from weak to strong coupling", Sci. Rep. 5, 11787 (2015).
- <sup>32</sup>G. D. Scholes, X. J. Jordanides, and G. R. Fleming, "Adapting the förster theory of energy transfer for modeling dynamics in aggregated molecular assemblies", J. Phys. Chem. B 105, 1640–1651 (2001).
- <sup>33</sup>S. Jang, "Theory of multichromophoric coherent resonance energy transfer: a polaronic quantum master equation approach", J. Chem. Phys. 135, 034105 (2011).
- <sup>34</sup>J. Ma and J. Cao, "Förster resonance energy transfer, absorption and emission spectra in multichromophoric systems. i. full cumulant expansions and system-bath entanglement", J. Chem. Phys. 142, 094106 (2015).
- <sup>35</sup>J. Ma, J. Moix, and J. Cao, "Förster resonance energy transfer, absorption and emission spectra in multichromophoric systems. ii. hybrid cumulant expansion", J. Chem. Phys. **142**, 094107 (2015).
- <sup>36</sup>J. M. Moix, J. Ma, and J. Cao, "Förster resonance energy transfer, absorption and emission spectra in multichromophoric systems. iii. exact stochastic path integral evaluation", J. Chem. Phys. 142, 094108 (2015).
- <sup>37</sup>S. Jang, Y.-C. Cheng, D. R. Reichman, and J. D. Eaves, "Theory of coherent resonance energy transfer", J. Chem. Phys. 129, 101104 (2008).
- <sup>38</sup>A. Ishizaki and G. R. Fleming, "On the adequacy of the redfield equation and related approaches to the study of quantum dynamics in electronic energy transfer", J. Chem. Phys. **130**, 234110 (2009).
- <sup>39</sup>A. Nazir, "Correlation-dependent coherent to incoherent transitions in resonant energy transfer dynamics", Phys. Rev. Lett. 103, 146404 (2009).

- <sup>40</sup>P. Huo and D. F. Coker, "Iterative linearized density matrix propagation for modeling coherent excitation energy transfer in photosynthetic light harvesting", J. Chem. Phys. **133** (2010).
- <sup>41</sup>P. Huo and D. F. Coker, "Theoretical study of coherent excitation energy transfer in cryptophyte phycocyanin 645 at physiological temperature", J. Phys. Chem. Lett. **2**, 825–833 (2011).
- <sup>42</sup>L.-Y. Hsu, W. Ding, and G. C. Schatz, "Plasmon-coupled resonance energy transfer", J. Phys. Chem. Lett. 8, 2357–2367 (2017).
- <sup>43</sup>B. Pettersson Rimgard, Z. Tao, G. A. Parada, L. F. Cotter, S. Hammes-Schiffer, J. M. Mayer, and L. Hammarström, "Proton-coupled energy transfer in molecular triads", Science 377, 742–747 (2022).
- <sup>44</sup>E. R. Sayfutyarova and S. Hammes-Schiffer, "Substituent effects on photochemistry of anthracene—phenol–pyridine triads revealed by multireference calculations", J. Am. Chem. Soc. **142**, 487–494 (2019).
- <sup>45</sup>E. R. Sayfutyarova and S. Hammes-Schiffer, "Excited state molecular dynamics of photoinduced proton-coupled electron transfer in anthracene-phenol-pyridine triads", J. Phys. Chem. Lett. 11, 7109–7115 (2020).
- <sup>46</sup>E. R. Young, J. Rosenthal, and D. G. Nocera, "Energy transfer mediated by asymmetric hydrogen-bonded interfaces", Chem. Sci. **3**, 455–459 (2012).
- <sup>47</sup>C. Drolen, E. Conklin, S. J. Hetterich, A. Krishnamurthy, G. A. Andrade, J. L. Dimeglio, M. I. Martin, L. K. Tran, G. P. Yap, J. Rosenthal, et al., "Ph-driven mechanistic switching from electron transfer to energy transfer between [ru(bpy)<sub>3</sub>]<sup>+</sup><sub>2</sub> and ferrocene derivatives", J. Am. Chem. Soc. **140**, 10169–10178 (2018).
- <sup>48</sup>A. Soudackov and S. Hammes-Schiffer, "Multistate continuum theory for multiple charge transfer reactions in solution", J. Chem. Phys. 111, 4672–4687 (1999).
- <sup>49</sup>A. Soudackov and S. Hammes-Schiffer, "Derivation of rate expressions for nonadiabatic proton-coupled electron transfer reactions in solution", J. Chem. Phys. 113, 2385–2396 (2000).
- <sup>50</sup>S. Hammes-Schiffer and A. V. Soudackov, "Proton-coupled electron transfer in solution, proteins, and electrochemistry", J. Phys. Chem. B 112, 14108–14123 (2008).
- <sup>51</sup>S. Hammes-Schiffer, "Proton-coupled electron transfer: moving together and charging forward", J. Am. Chem. Soc. 137, 8860–8871 (2015).

- <sup>52</sup>D. V. Matyushov and G. A. Voth, "Modeling the free energy surfaces of electron transfer in condensed phases", J. Chem. Phys. 113, 5413–5424 (2000).
- <sup>53</sup>D. W. Small, D. V. Matyushov, and G. A. Voth, "The theory of electron transfer reactions: what may be missing?", J. Am. Chem. Soc. 125, 7470–7478 (2003).
- <sup>54</sup>M. M. Waskasi, M. D. Newton, and D. V. Matyushov, "Impact of temperature and non-gaussian statistics on electron transfer in donor-bridge-acceptor molecules", J. Phys. Chem. B 121, 2665– 2676 (2017).
- <sup>55</sup>R. Zwanzig, Nonequilibrium statistical mechanics (Oxford University Press, 2001).
- <sup>56</sup>M. Cho and R. J. Silbey, "Nonequilibrium photoinduced electron transfer", J. Chem. Phys. 103, 595–606 (1995).
- <sup>57</sup>D. C. Borgis, S. Lee, and J. T. Hynes, "A dynamical theory of nonadiabatic proton and hydrogen atom transfer reaction rates in solution", Chem. Phys. Lett. **162**, 19–26 (1989).
- <sup>58</sup>D. Borgis and J. T. Hynes, "Dynamical theory of proton tunneling transfer rates in solution: general formulation", Chem. Phys. **170**, 315–346 (1993).
- <sup>59</sup>A. Soudackov, E. Hatcher, and S. Hammes-Schiffer, "Quantum and dynamical effects of proton donor-acceptor vibrational motion in nonadiabatic proton-coupled electron transfer reactions", J. Chem. Phys. **122**, 014505 (2005).
- <sup>60</sup>A. Sirjoosingh and S. Hammes-Schiffer, "Proton-coupled electron transfer versus hydrogen atom transfer: generation of charge-localized diabatic states", J. Phys. Chem. A 115, 2367–2377 (2011).
- <sup>61</sup> J. H. Skone, A. V. Soudackov, and S. Hammes-Schiffer, "Calculation of vibronic couplings for phenoxyl/phenol and benzyl/toluene self-exchange reactions: implications for proton-coupled electron transfer mechanisms", J. Am. Chem. Soc. 128, 16655–16663 (2006).
- <sup>62</sup>Y. Georgievskii and A. A. Stuchebrukhov, "Concerted electron and proton transfer: transition from nonadiabatic to adiabatic proton tunneling", J. Chem. Phys. 113, 10438–10450 (2000).
- <sup>63</sup>S. E. Braslavsky, E. Fron, H. B. Rodríguez, E. S. Román, G. D. Scholes, G. Schweitzer, B. Valeur, and J. Wirz, "Pitfalls and limitations in the practical use of förster's theory of resonance energy transfer", Photochem. Photobiol. Sci. 7, 1444–1448 (2008).
- <sup>64</sup>G. D. Scholes and K. P. Ghiggino, "Electronic interactions and interchromophore excitation transfer", J. Phys. Chem. 98, 4580–4590 (1994).

- <sup>65</sup>C.-P. Hsu, "The electronic couplings in electron transfer and excitation energy transfer", Acc. Chem. Res. 42, 509–518 (2009).
- <sup>66</sup>Z.-Q. You, C.-P. Hsu, and G. R. Fleming, "Triplet-triplet energy-transfer coupling: theory and calculation", J. Chem. Phys. **124** (2006).
- <sup>67</sup>C. C. Marston and G. G. Balint-Kurti, "The fourier grid hamiltonian method for bound state eigenvalues and eigenfunctions", J. Chem. Phys. 91, 3571–3576 (1989).
- <sup>68</sup>V. Barone, J. Bloino, M. Biczysko, and F. Santoro, "Fully integrated approach to compute vibrationally resolved optical spectra: from small molecules to macrosystems", J. Chem. Theory Comput. 5, 540–554 (2009).
- <sup>69</sup>J. Bloino, M. Biczysko, F. Santoro, and V. Barone, "General approach to compute vibrationally resolved one-photon electronic spectra", J. Chem. Theory Comput. 6, 1256–1274 (2010).
- <sup>70</sup>Z. Murtaza, D. K. Graff, A. P. Zipp, L. A. Worl, W. E. J. Jones, W. D. Bates, and T. J. Meyer, "Energy transfer in the inverted region: calculation of relative rate constants by emission spectral fitting", J. Phys. Chem. 98, 10504–10513 (1994).
- <sup>71</sup>Z. K. Goldsmith, A. V. Soudackov, and S. Hammes-Schiffer, "Theoretical analysis of the inverted region in photoinduced proton-coupled electron transfer", Farad. Disc. 216, 363–378 (2019).
- <sup>72</sup>G. A. Parada, Z. K. Goldsmith, S. Kolmar, B. Pettersson Rimgard, B. Q. Mercado, L. Hammarström, S. Hammes-Schiffer, and J. M. Mayer, "Concerted proton-electron transfer reactions in the marcus inverted region", Science 364, 471–475 (2019).
- <sup>73</sup>X. J. Jordanides, G. D. Scholes, and G. R. Fleming, "The mechanism of energy transfer in the bacterial photosynthetic reaction center", J. Phys. Chem. B 105, 1652–1669 (2001).